






Article

The Lowermost Tejo River Terrace at Foz do Enxarrique, Portugal: A Palaeoenvironmental Archive from c. 60–35 ka and Its Implications for the Last Neanderthals in Westernmost Iberia

Pedro P. Cunha ^{1,*}, António A. Martins ², Jan-Pieter Buylaert ³, Andrew S. Murray ⁴,
Maria P. Gouveia ¹, Eric Font ^{5,6}, Telmo Pereira ⁷, Silvério Figueiredo ⁸,
Cristiana Ferreira ⁹, David R. Bridgland ¹⁰, Pu Yang ¹, José C. Stevaux ¹¹ and Rui Mota ¹

¹ MARE—Marine and Environmental Sciences Centre, Department of Earth Sciences, University of Coimbra, Rua Sílvio Lima, Univ. Coimbra—Pólo II, 3030-790 Coimbra, Portugal; mariamporto@gmail.com (M.P.G.); pu.yang991@gmail.com (P.Y.); ruimota16@gmail.com (R.M.)

² ICT—Instituto de Ciências da Terra, Departamento de Geociências, Universidade de Évora, Rua Romão Ramalho, 59, 7000-671 Évora, Portugal; aam@uevora.pt

³ Centre for Nuclear Technologies, Technical University of Denmark, DTU Risø Campus, DK-4000 Roskilde, Denmark; jabu@dtu.dk

⁴ Nordic Laboratory for Luminescence Dating, Aarhus University, DTU Risø Campus, DK-4000 Roskilde, Denmark; anmu@dtu.dk

⁵ IDL-FCUL, Instituto Dom Luís, Faculdade de Ciências da Universidade de Lisboa, Campo Grande, 1749-016 Lisboa, Portugal; font_eric@hotmail.com

⁶ Department of Earth Sciences, University of Coimbra, Rua Sílvio Lima, Univ. Coimbra—Pólo II, 3030-790 Coimbra, Portugal

⁷ ICArEHB—Interdisciplinary Center for Archaeology and Evolution of Human Behaviour, Faculdade de Ciências Humanas e Sociais, Universidade do Algarve, Campus da Penha, 8005-139 Faro, Portugal; telmojrperreira@gmail.com

⁸ Geosciences Center—U.C., Portuguese Center of Geo-History and Prehistory, Polytechnic Institute of Tomar, Quinta do Contador, Estrada da Serra, 2300-313 Tomar, Portugal; silverio.figueiredo@ipt.pt

⁹ Geosciences Center—U.C., Portuguese Center of Geo-History and Prehistory, Earth and Memory Institute, 6120-721 Mação, Portugal; ferreira.cris.00@gmail.com

¹⁰ Department of Geography, Durham University, South Road, Durham DH1 3LE, UK; d.r.bridgland@durham.ac.uk

¹¹ Universidade Federal de Mato Grosso do Sul/Camus, Avenida Ranulpho Marques Leal, 3484, Três Lagoas 76620-080, MS, Brazil; josecstevaux@gmail.com

* Correspondence: pcunha@dct.uc.pt

Academic Editors: Jef Vandenberghe and Valentí Rull

Received: 11 October 2018; Accepted: 11 January 2019; Published: 18 January 2019



Abstract: Reconstruction of Pleistocene environments and processes in the sensitive geographical location of westernmost Iberia, facing the North Atlantic Ocean, is crucial for understanding impacts on early human communities. We provide a characterization of the lowest terrace (T6) of the Lower Tejo River, at Vila Velha de Ródão (eastern central Portugal). This terrace comprises a lower gravel bed and an upper division consisting of fine to very fine sands and coarse silts. We have used a multidisciplinary approach, combining geomorphology, optically stimulated luminescence (OSL) dating, grain-size analysis and rock magnetism measurement, in order to provide new insights into the environmental changes coincident with the activity of the last Neanderthals in this region. In addition, we conducted palynological analysis, X-ray diffraction measurement and scanning electron microscopy coupled with energy dispersive spectra of the clay fraction and carbonate concretions. We discuss these new findings in the context of previously published palaeontological and archeological data. The widespread occurrence of carbonate concretions and rizoliths in the T6 profile is evidence for episodic pedogenic evaporation, in agreement with the rare occurrence

and poor preservation of phytoliths. We provide updated OSL ages for the lower two Tejo terraces, obtained by post infra-red stimulated luminescence: (i) T5 is c. 140 to 70 ka; (ii) T6 is c. 60 to 35 ka. The single archaeological and fossiliferous level located at the base of the T6 upper division, recording the last regional occurrence of megafauna (elephant and rhinoceros) and Mousterian artefacts, is now dated at 44 ± 3 ka. With reference to the arrival of Neanderthals in the region, probably by way of the Tejo valley (from central Iberia), new dating suggests a probable age of 200–170 ka for the earliest Mousterian industry located in the topmost deposits of T4.

Keywords: OSL dating; river terraces; Late Pleistocene; environmental change; western Iberia

1. Introduction

The Vila Velha do Ródão and Arneiro depressions are located in the furthest upstream reach of the Lower Tejo River, about 20 km from the Spanish border (this is Portuguese Reach I as defined by reference [1]) (Figure 1). From the sensitive location of the study area close to the North Atlantic, we can assume strong interaction between marine and terrestrial processes and environmental conditions. This highlights the relevance of this area for research on past climate and environmental change. Previous research in the study area has mainly focused on characterizing the geological setting, geomorphic genesis (e.g., of the terrace staircase), active tectonics, archaeological background and landscape evolution in general (e.g., see review in reference [2]). Climatic and environmental changes in the Lower Tejo Basin during the last glacial cycle and especially during Marine Isotope Stage (MIS) 3, remain poorly documented.

The Middle Palaeolithic of Iberia has received considerable attention in recent times in connection with the extinction of the Neanderthals [3–15], but is also relevant in connection with the early establishment of the Mousterian, the diversity and demise of early hominins and the widespread distribution of the first Neanderthals [16–21].

Since the 1970s, 37 archaeological contexts in the study area have been recorded, ranging from Acheulean to Mesolithic; amongst these, 17 are small surface assemblages of uncharacteristic chopper-like cores and flakes, broadly assigned to the Palaeolithic, and eight were obtained from excavation [22] (Foz do Enxarrique, Vilas Ruivas, Pegos do Tejo-2, Azinhal, Tapada do Montinho, Cobrinhos, Monte da Revelada and Alto da Revelada) (Figure 1).

In this contribution, we focus on the sedimentary record from the lowest terrace (T6) of the Tejo at Vila Velha de Rodão, which represents an important terrestrial archive of relevance to the possible relation between palaeoenvironmental conditions and early human occupation dynamics in the region. Herein, we reconstruct and discuss the climate and environmental conditions during the last glacial cycle, through integration of evidence from optically stimulated luminescence (OSL) dating, grain-size distribution, rock magnetic properties (low field magnetic susceptibility, frequency-dependent magnetic susceptibility and isothermal remanent magnetization curves), sediment mineralogy, phytoliths and palynology, as well as reviewing published paleontological and archaeological data.

2. Geological and Geomorphological Setting

The Tejo is one of the largest systems of Western Europe and flows E–W across almost the whole of Iberia; it is an ancient river (c. 3.7 Ma) with an important sedimentary record [23,24]. In the uppermost Portuguese reach of the Lower Tejo, the river flows through two quartzite ridges by way of the Ródão gorge (named “Portas de Ródão”), which separates the Ródão (upstream) and Arneiro (downstream) depressions.

The oldest bedrock comprises the Neoproterozoic and lower Cambrian schists and metagreywackes of the Beiras Group and the Ordovician Armorican Quartzite Formation. The latter is dominated by resistant ridges that topographically dominate (by c. 150 m) the extensive adjacent

planation surface developed on phylites and metagreywackes. The Cenozoic is represented by the Cabeço do Infante Formation, the Silveirinha dos Figos Formation and the Murracha Group. The first two are dominated by soft sandstones and gravels, while the Murracha Group consists of gravels interbedded with fine sediments [23,25].

In Lower Tejo Reach I, below a culminant sedimentary unit (the Falagueira Formation, at c. +260 m—above the river bed) corresponding to the ancestral Tejo River before drainage network entrenchment, the Pleistocene to Holocene record is summarized as follows [1,2,26] (Figure 1): (i) T1, with the surface at +111 m, without artefacts; (ii) T2, at +83 m, without artefacts; (iii) T3, at +61 m, without artefacts; (iv) T4, at +34 m, with Acheulean in the basal and middle levels and Mousterian in the uppermost levels; (v) T5, at +18 m, with Mousterian industries through the entire fluvial sequence; (vi) T6, at +10 m, with Mousterian industries at the lower deposits; (vii) Carregueira Formation (aeolian sands) (32 to 12 ka), with Upper Palaeolithic to Epi-Palaeolithic industries; (viii) Alluvial plain and a cover unit of aeolian sands (Holocene), with Mesolithic and more recent industries. Immediately upstream of the Ródão gorge, the modern river bed is at c. 72 m above sea level (a.s.l.). In this area, geomorphological evidence for late Cenozoic tectonics arises from interpretation of valley asymmetry and drainage patterns, fault scarps, tectonic lineaments, fracture-controlled valleys, and vertical displacement of planation surfaces and terraces [26]. The sedimentary controls for the formation of the Lower Tejo terrace staircase (mainly glacio-eustasy and differential uplift) are different from those affecting the Middle and Upper Tejo, because of separation (between the Middle and Lower Tejo) by a lengthy knick zone through hard basement [27,28].

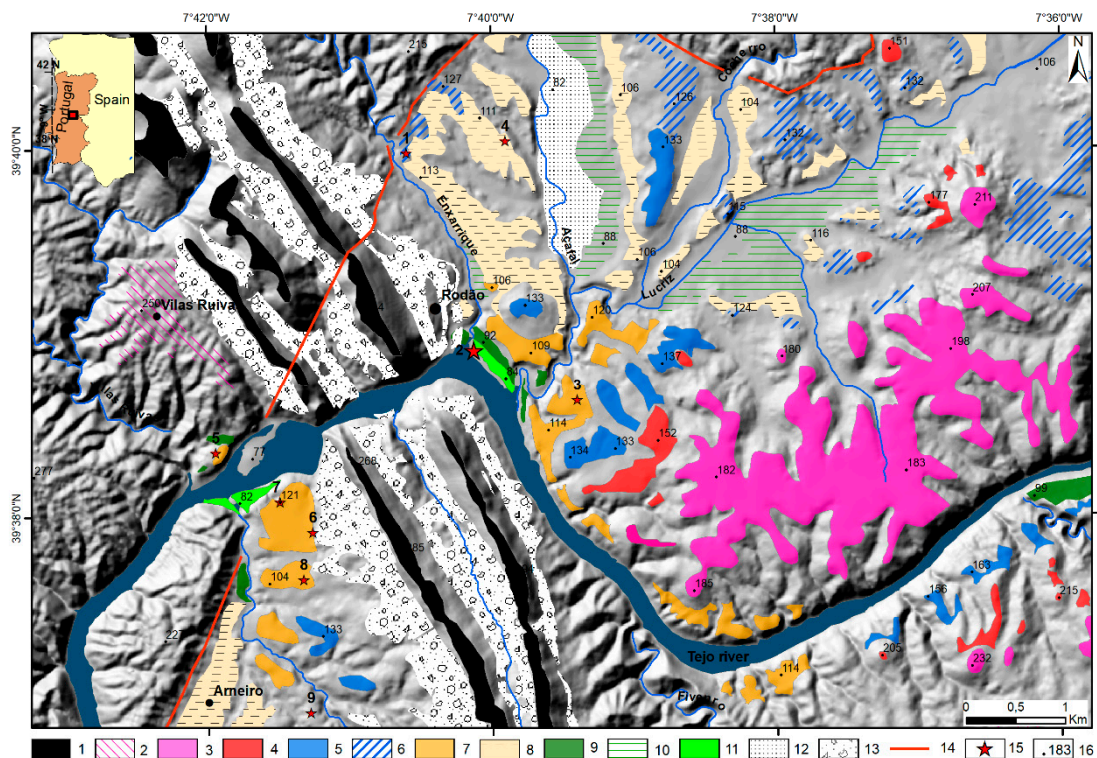


Figure 1. Geomorphological map of Lower Tejo Reach I (Vila Velha de Ródão and Arneiro depressions): 1—quartzite ridge; 2—erosion level (a strath without sedimentary deposits) correlative with T1; 3—T1; 4—T2; 5—T3; 6—erosion level correlative with T3; 7—T4; 8—erosion level correlative with T4; 9—T5; 10—erosion level correlative with T5; 11—T6; 12—alluvial plain; 13—colluvium; 14—Ponsul fault; 15—archaeological sites; 16—altitude (m). Palaeolithic sites: 1—Cobrinhos; 2—Foz do Enxarrique; 3—Monte do Famaco; 4—Monte da Revelada and Alto da Revelada; 5—Vilas Ruivas; 6—Tapada do Montinho; 7—Pegos do Tejo-2; 8—Arneiro; 9—Azinhal.

Previous dating of the Pleistocene lithostratigraphic divisions was undertaken using Uranium-series, Thermoluminescence (TL), Optically stimulated luminescence on quartz (Quartz-OSL) and infra-red stimulated luminescence (IRSL) on K-feldspar. Quartz-OSL was used to date: the Carregueira Formation (32 to 12 ka; 3 ka) [2]; the alluvial deposits at the Azinhal archaeological site, linked to T6 (61 ± 2 ka: GLL code 050302); the topmost deposits of T4 at the Pegos do Tejo-2 archaeological site (minimum age of 135 ± 21 ka: GLL code 050301) [29]. In Reach I of the Tejo, IRSL dating provided a first temporal framework for the Lower Tejo terraces [26], but at that stage of research T5 and T6 were not yet separated as distinct terraces. Recently, T4 in Lower Tejo Reach IV was dated to c. 340 to 155 ka, using post infra-red stimulated luminescence (pIRIR) [28].

3. Methods

Geomorphological, stratigraphical, sedimentological and chronological data were obtained using standard methodology (e.g., [30]): (1) geomorphological study, complemented by local detailed investigations and the production of a detailed map using Geographic Information System (GIS), (2) field descriptions of the sedimentary units, (3) sedimentological characterization of the deposits and (4) luminescence dating.

3.1. Geomorphological Mapping

Geomorphological mapping was undertaken in three stages: (1) field mapping onto topographical (1/25,000) and geological (1/50,000) base maps, (2) analysis of 1/25,000 aerial photographs and of a digital elevation model (DEM) based upon a 1/25,000 and 1/10,000 topographic databases and (3) field ground truthing.

3.2. Field Work

The T6 deposits at Foz do Enxarrique were studied in detail in order to improve our understanding of the local stratigraphy and sedimentology. Exposures of T5 and T4 in the study area were also revisited. Fieldwork included stratigraphic logging and sedimentological characterization of the sedimentary deposits in order to obtain data on the depositional facies, including sediment colour, texture, maximum particle size, clast lithology, fossil content, bedding and depositional architecture.

At the studied stratigraphic section of T6 at Foz do Enxarrique, continuous sediment sampling was undertaken manually, every 1 cm, to a depth of 5.00 m. Samples were labelled as follows: e.g., for "T6FE0.21", T6 identifies the terrace code, FE the site and 0.21 the sample depth. We also collected a present-day sediment sample from the Foz do Enxarrique stream bed (FE-modern). Each sampled horizon (1 cm) was characterised according to its colour (using the Munsell system), texture and the relative abundance of carbonate concretions. Phytolith analyses were undertaken on carbonate concretions from five levels within the sequence (T6FE0.72, T6FE2.00, T6FE2.46–2.48, T6FE3.48 and T6FE5.00). An additional seven samples (spanning greater depth) were collected for clay mineralogy and palynological studies (T6FE0.70–0.74, T6FE1.13–1.17, T6FE1.98–2.02, T6FE2.88–2.92, T6FE3.46–3.50, T6FE4.10–4.14 and T6FE4.49–4.52). Palynological study also included samples collected from the T6 archaeological level with fossil bones: codes T6FE/15 0.25–0.30, T6FE/15 0.35–0.40 and T6FE/15 0.45–0.50 (here, the depth refers to the top of the archaeological level). The T6 upper unit at Foz do Enxarrique was sampled for optically stimulated luminescence (OSL) dating: sample 062201 collected at 0.89–0.93 m depth (below the terrace surface); sample 052202 collected at a 5.20–5.30 m depth; sample 052201 collected at a 5.40–5.50 m depth (top of the archaeological and fossiliferous layer).

At the Foz do Enxarrique site, a 1 m thick exposure reveals the lower part of T5. Two samples (T5FE0.15–0.23 and T5FE0.92–1.00) were collected here for clay mineralogy and palynological studies. At this site, two further samples for OSL dating (052204 and 052247) were collected at depths of 1.50 and 2.00 m below the T5 surface. T5 was also sampled for OSL dating at the Vilas Ruivas site (052207, 052231 and 052253).

From T4, samples for OSL dating were obtained from the Vilas Ruivas, Rodense Bolaria (Vila Velha de Ródão) and Pegos do Tejo-2 (Arneiro) sites (Figure 1).

3.3. Optically Stimulated Luminescence Dating

From Reach I of the Lower Tejo, samples for OSL dating were previously collected from the sedimentary successions of the T4, T5 and T6 terraces and dated by IRSL, with a correction for the anomalous fading effect [26], because the quartz-OSL signal was found to be in saturation. However, it was later documented that the fading correction used was inappropriate, leading to age underestimation. In order to improve the chronology of the terrace sequences and their associated lithic industries, we now use the pIRIR protocol. K-feldspar grains from the samples dated in 2008 (IRSL) were measured (Equivalent doses) in 2013 by pIRIR (the most up-to-date protocol); these new results are now presented. The storage of K-feldspar grains does not affect the luminescence properties or the resulting ages. In summary, several samples were selected for OSL dating (pIRIR protocol): three from T6 at Foz do Enxarrique (upper unit), five from T5 (collected at Foz do Enxarrique and Vilas Ruivas; Figure 1) and four from T4 (collected at Pegos do Tejo-2, Vilas Ruivas and Rodense Bolaria/V.V.Ródão; Figure 1).

OSL is an absolute dating technique that measures the time elapsed since sedimentary quartz or feldspar grains were last exposed to daylight [31]. Exposure to daylight during sediment transport removes the latent luminescence signal from those minerals. After burial, the luminescence signal (trapped charge) starts to accumulate in the mineral grains due to ionising radiation. The annual dose of a sediment sample is related to the decay of ^{238}U , ^{232}Th and ^{40}K present in the sediment itself, to cosmic ray bombardment and to the water content of the sediment. In the laboratory, the equivalent dose (D_e , assumed to be the dose absorbed since the last exposure to light, i.e., the burial dose, expressed in Grays—Gy) is determined by comparing the natural luminescence signal resulting from charge trapped during burial with that trapped during a laboratory irradiation. In this study, the radionuclide concentrations were measured by high-resolution gamma spectrometry [32]. These concentrations were then converted to environmental dose rates using the specified conversion factors [33]. For the calculation of the dose rate of sand-sized K-feldspar grains, an internal K content of $12.5 \pm 0.5\%$ was assumed [34]. Dividing the D_e by the environmental dose rate (in Gy/ka) gives the luminescence age of the sediment.

Sample preparation for luminescence analyses was carried out in darkroom conditions, at the Department of Earth Sciences of the University of Coimbra. Samples were wet-sieved to separate the 180–250 μm grain-size fraction, followed by HCl (10%) and H_2O_2 (10%) treatments to remove carbonates and organic matter, respectively. The K-feldspar-rich fraction was floated off using a heavy liquid solution of sodium polytungstate ($\rho = 2.58 \text{ g/cm}^3$). The K-feldspar fraction was treated with 10% HF for 40 min to remove the outer alpha-irradiated layer and to clean the grains. After etching, the fraction was treated with HCl (10%) to dissolve any remaining fluorides.

At the Nordic Laboratory for Luminescence Dating (NLL), OSL were conducted using automated luminescence Risø TL/OSL-20 readers (Roskilde, Denmark), each containing a calibrated beta source. Small (2 mm) aliquots of K-feldspar were mounted in stainless steel cups. The K-feldspar equivalent doses (D_e) were measured with a pIRIR SAR protocol using a blue filter combination [35,36]. Preheating was at 320 °C for 60 s and the cut-heat 310 °C for 60 s. After preheating the aliquots were IR bleached at 50 °C for 200 s (IR₅₀ signal) and subsequently stimulated again with IR at 290 °C for 200 s (pIRIR₂₉₀ signal). It has been shown [36] that the post-IR IRSL signal measured at 290 °C can give accurate results without the need to correct for signal instability. For all IR₅₀ and pIRIR₂₉₀ calculations, the initial 2 s of the luminescence decay curve less a background derived from the last 50 s was used.

3.4. Grain-Size Measurements

Grain-size analyses of uncemented sediment samples was carried out using a Beckman Coulter LS230 laser granulometer (Brea, CA, USA), with a measurement range of 0.04 to 2000 μm and a

relative error less than 2%. Visual inspection of grain-size distribution curves allowed the identification and interpretation of unimodal or multimodal subpopulations. The T6FE sediment samples of the 5.00–3.20 m depth interval were analysed at a 5 cm spacing; the 3.18–2.60 m and 2.50–0.30 m depth intervals were analysed at a 1 cm spacing in order to provide a better distinction between fluvial and aeolian deposition.

3.5. Mineral Composition

Analyses of sediment composition were based on binocular microscope observation and X-ray diffraction (Department of Earth Sciences—University of Coimbra), as well as Scanning Electron Microscopy (SEM) and Energy Dispersive Spectrometry (EDS) of selected carbonate concretions (UNESP Laboratory, at the University of Rio Claro—Brazil). A Philips PW 3710 X-ray diffractometer (Virginia, USA), with a Cu tube, at 40 kV and 20 nA was used for mineralogical identification within carbonate concretions and for clay mineralogy. The mineralogical composition of the <2 µm fraction was obtained in oriented samples before and after ethylene glycol treatment and heating up to 550 °C. The percentages of the clay minerals in each sample were determined through the peak areas of the mineral present, with the use of specific correction parameters.

3.6. Rock Magnetism

For magnetic susceptibility measurement, samples were dried at 40 °C and transferred into plastic bags for subsequent analysis. Rock magnetic properties were measured in the Instituto Dom Luis, University of Lisboa and in the Department of Earth Sciences of the University of Coimbra, and consisted of low field mass specific magnetic susceptibility (χ in m³/kg), frequency-dependent magnetic susceptibility (K_{fd} in %) and isothermal remnant magnetization (IRM). Magnetic susceptibility measures the ability of a material to be magnetized and includes contributions (in proportion to their abundance) from all diamagnetic (calcite), paramagnetic (clays), and ferromagnetic (magnetite) minerals present in the sediment. Low-field magnetic susceptibility was measured with a MFK1 (AGICO Inc, Brno, Czech Republic) apparatus operating with magnetic field intensity of 200 A/m and frequency of 978 Hz. Data were reported as mass-normalized values (m³/kg). Frequency-dependent magnetic susceptibility is an indicator of the presence of superparamagnetic particles (SP), generally produced during pedogenic processes. Low (0.47 kHz) and high (4.7 kHz) frequency-dependent magnetic susceptibility was measured with a Bartington Instruments magnetic susceptibility meter coupled to a MS2B sensor and reported in percentage as follows: $K_{fd} (\%) = 100 \cdot (K_{lf} - K_{hf}) / K_{lf}$. After cleaning by alternating field demagnetization up to 100 mT, samples were subsequently submitted to stepwise isothermal remanent magnetization (IRM) acquisition with an impulse magnetizer (model IM-10-30). We applied maximum fields of 1.2T following approximately 30 steps. Remanence was measured with a JR-6A (AGICO Inc, Brno, Czech Republic) magnetometer.

Data were analysed using a cumulative log-Gaussian (CLG) function with software developed for the purpose [37]. The S-ratio was calculated with the formula $-IRM_{-0.3T} / IRM_{1T}$.

3.7. Phytoliths

For phytolith analyses, samples with a volume of 1 cm³ were placed in an Erlenmeyer flask and dissolved in 20 mL of HNO₃ and H₂SO₄ solution at 1:4. The material was heated for 3 h at 90 °C on a hot plate. After cooling at ~25 °C, 10 ml of H₂O₂ was added, before washing in distilled water, centrifuging (1500 rotations per minute up to neutralization (pH ~ 7.0), and washing with alcohol. For slide preparation, 50 µL of material was extracted by pipette, placed on slides and dried on hot plates. Coverslips were fixed using Entelan[®] resin (Hatfield, UK). Phytoliths were analyzed through optical microscopy (×160 and ×640), identified with reference to literature [38–40] and named according to the International Code of Phytolith Nomenclature [41].

3.8. Palynology

For palynological studies, thirteen sediment samples were selected: two from lower and middle levels within T5; three from the T6 archaeological level and eight samples from the upper division of T6 (silty very fine sands and sandy silts). These samples were subjected to a physical and chemical pollen concentration pre-treatment. The pollen residue was isolated with a standard palynological preparation methodology [42], with some modifications: omitting acetolysis and sieving, the latter in an attempt to increase pollen concentration. The pollen residue was assembled on thin glass slides to allow its identification and counting. It was embedded in glycerine and sealed with histolaque, to permit movement of the grains for more complete observation of the morphological features of pollen and non-pollen-palynomorphs. Grains were identified (based on references [43–46]) and counted using an optical transmitted-light microscope.

3.9. Geochemical Analyses

Geochemical analyses on sediment samples collected from the upper unit of T6 were performed, at the laboratory, with a X-ray fluorescence spectrometer (Niton XL3t Ultra Analyser—Thermo Fisher Scientific; Waltham, MA, USA).

4. Results

4.1. Geomorphology, Lithostratigraphy and Sedimentology

In the confluence area of the Enxarrique stream with the Tejo, several geomorphic units are represented: T1, at 179 m a.s.l.; T2, at 149 m a.s.l.; T3, at 132 m a.s.l.; T4, at 106 m a.s.l.; T5, at 89 m a.s.l.; T6, at 83 m a.s.l.; alluvial plain of the Açafal stream, at 78 m a.s.l. (Figure 2).

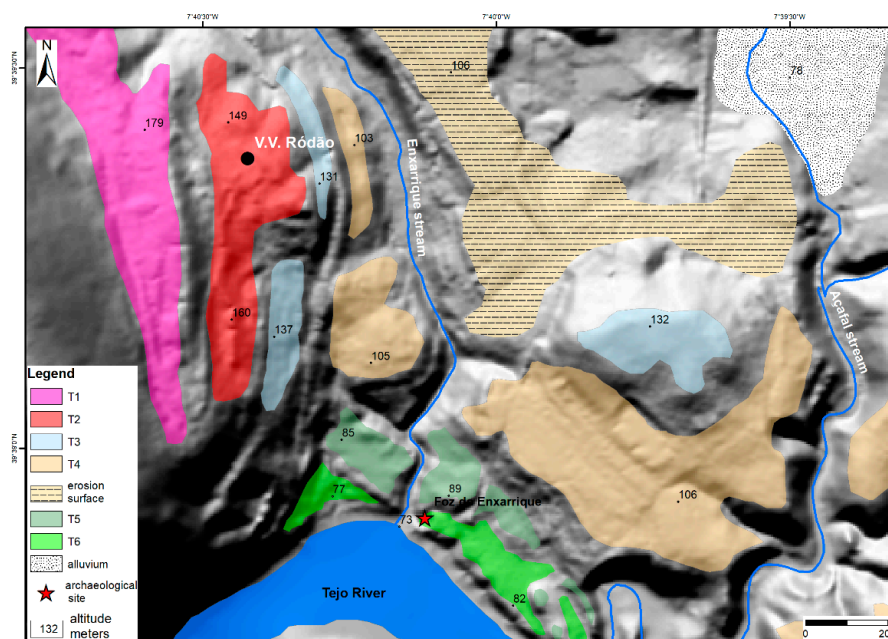


Figure 2. Geomorphological map of the neighbourhood of the Foz do Enxarrique site (Vila Velha de Ródão). This digital elevation model was performed with 2 m of equidistant contours and pixels of 5×5 m. The fluvial terraces, numbered from higher (T1) to lower (T6), are disposed in a staircase. The mapped erosion surface (a strath without sedimentary deposits) correlates with the T4 terrace. The location of the Foz do Enxarrique archaeological site is indicated.

In the Vila Velha de Ródão—Arneiro area, T4 comprises a lower boulder gravel (up to 2 m-thick) and an upper division of gravelly coarse sands (up to 2 m thick). The main exposures are at Pegos do

Tejo-2 and Vilas Ruivas, both located in the Arneiro depression (Figure 1). The massive clast-supported boulder gravel comprises clasts that are subrounded, with MPS (mean diameter of the 10 largest clasts) = 32 cm, of quartzite (75%), white quartz and rare slates/metagreywackes.

The T5 terrace usually has a basal gravelly pavement (c. 0.2 m thick) overlain by very fine sands (up to 2.3 m thick), with some very thin (<1 cm) levels containing calcium carbonate concretions. The main outcrops are provided by the sites at Foz do Enxarrique (up to c. 2.5 m thick) and Vilas Ruivas (0.5 m thick).

The sedimentary deposits of T6 are well exposed at the Foz do Enxarrique site (Figures 2–4) and were studied in detail during the work reported here. The sedimentary infill of T6 comprises a lower gravel, up to 0.40 m thick, and an upper unit, c. 5.60 m thick, dominated by very fine sands and coarse silts.



Figure 3. View of the T6 section at the Foz do Enxarrique archaeological site, with sampling underway. The surface of the T6 terrace is at 82 m a.s.l.; the exposures show the full thickness of the upper unit. The lower artificial pavement is placed approximately at the top of the bed containing artefacts and fossil bones (the archaeological level); the lower gravel bed is located just below this. A metal staircase and a platform has been built in front of the exposed section and provides access to the top as well some protection for the exposure. Note one of the several explanatory panels provided at the site. The Tejo River can be seen in the right background.

The upper unit of T6, generally lacking bedding but with rare lamination, can be divided into three layers: (i) from the surface to a depth of 4.55 m, an upper bed comprising sandy silts; (ii) from 4.55 to c. 5.40 m, a middle division consisting of micaceous very fine to fine sands with some interbedded thin gravel stringers; (iii) from c. 5.40–5.60 m, a bed comprising Mousterian artefacts and fossil bones in a matrix of micaceous fine sands. The predominant colour of the T6 upper unit deposits is yellowish brown to bright brown. The thin (1–3 cm thick) levels with calcium carbonate concretions and rhizoliths (Figure 5), 1–2 cm wide, are intercalated between thick intervals of uncemented sediment. At the depths of 4.55–4.57 and 4.73–4.82 m, quartzite and quartz clasts (<0.5 cm and <10 cm in size, respectively) and rolled concretions were observed dispersed in micaceous very fine to fine sands. A massive calcium carbonate level is present at a depth of 5.33–5.36 m, just above laminated fine sand. The levels containing calcium carbonate concretions do not show evidence of any erosive surface and they dip (up to 5 degrees) toward the Tejo River, progressively increasing in thickness.

The lower bed T6 consists of clast-supported boulder–pebble gravels, c. 0.4 m thick. The maximum clast diameter is 40 cm, with MPS = 31 cm. The gravel clast lithologies are quartzite (58%), milky quartz (27%) and metagreywakes/phylites (15%). The clasts are sub-rounded to angular. At about 76 m a.s.l., the T6 deposits overlie metamorphic basement, by an unconformity.

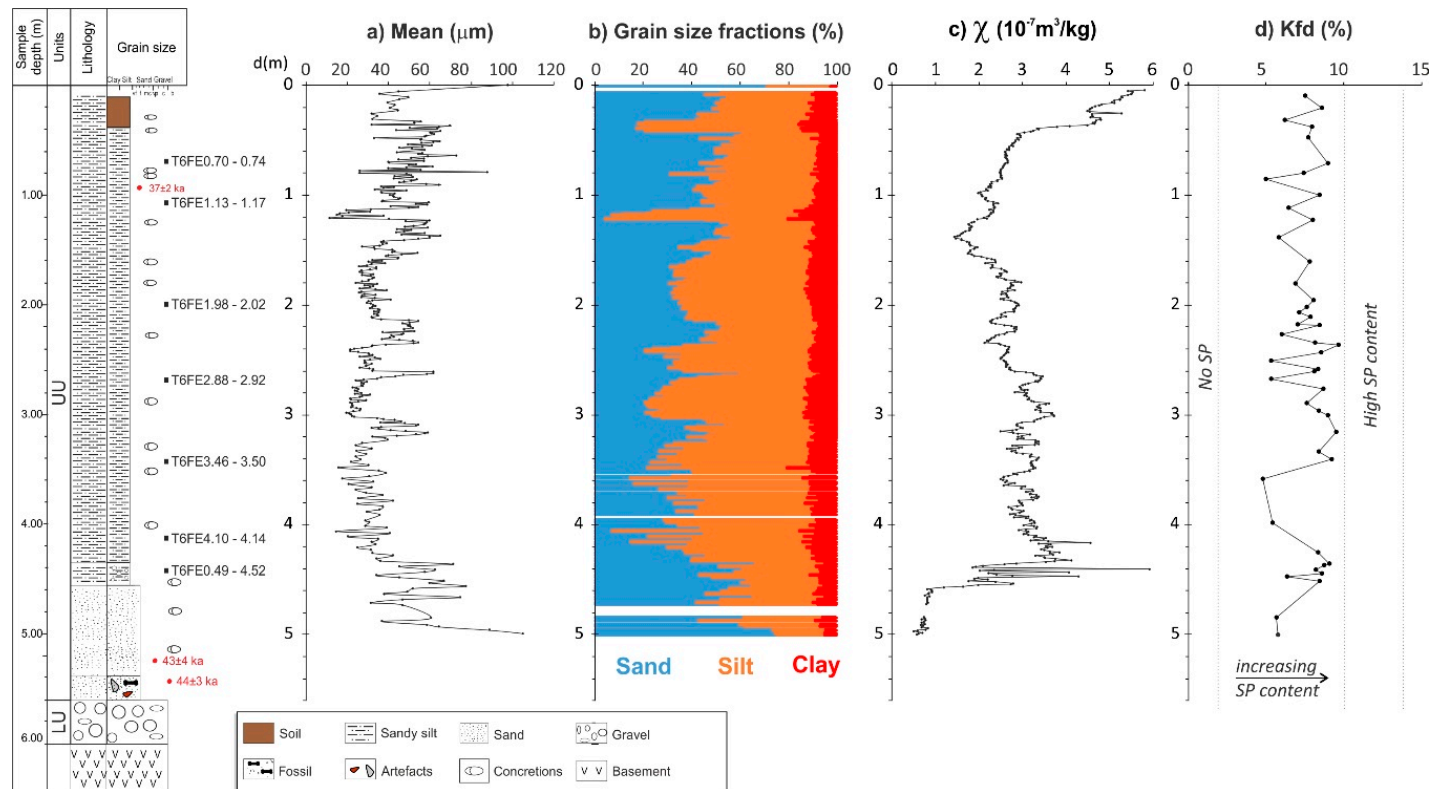


Figure 4. Stratigraphic log of the T6 terrace sequence at the Foz do Enxarrique archaeological site, also showing the (a) mean grain-size diameter, (b) main grain-size fractions in % (sand, 2000 to 63 μm; silt, 63 to 4 μm; clay, <4 μm), (c) mass specific magnetic susceptibility (χ) and (d) frequency-dependent magnetic susceptibility (Kfd in %), indicative of supermagnetic particles (SP). Black squares beside the stratigraphic log correspond to the sample intervals where palynological analysis and identification of clay minerals were conducted. Red circles indicate the stratigraphic location of optically stimulated luminescence (OSL) dated samples, with ages shown. LU—lower unit (gravels); UU—upper unit (dominated by very fine sands and coarse silts).



Figure 5. Examples of calcium carbonate concretions occurring in the coarse silts of T6: (A) three concretions collected, respectively, from depths of 3.56, 3.57 and 3.60 m; (B) a 2.5 cm thick concretion, obtained from a depth of 3.91–3.93 m; (C) two concretions and an agglomerate of two quartz pebbles, collected from a level at a depth of 4.73–4.83 m; (D) fragment of a quite continuous caliche level, 3 cm thick, that occurs at a depth of 5.33–5.36 m; (E) a 1 cm thick rhizolith, collected from a depth of 3.91–3.93 m.

4.2. Luminescence Dating Results

The luminescence dating results of the samples collected from T6, T5 and T4 are summarized in Tables 1 and 2. The geographical and stratigraphic locations of each sample are provided by Table 2. Four out of the twelve samples have D_e values lying above $2xD_0$ (corresponding to 86% of luminescence saturation). In view of the possibility of small systematic errors in the measurement of the luminescence signal, we feel it prudent to adopt the strategy of only presenting minimum doses for these samples (equivalent to $2xD_0$) and the derived minimum ages [47].

Table 1. Burial depth, Radionuclide activities (^{238}U , ^{226}Ra , ^{232}Th and ^{40}K) and water content used for dose-rate calculations of the luminescence dating samples.

NLL and Field Codes	X-Y Coordinates	U-238 (Bq kg ⁻¹)	Ra-226 (Bq kg ⁻¹)	Th-232 (Bq kg ⁻¹)	K-40 (Bq kg ⁻¹)	Water Content (%)
052201 PC1	39°58'59" N 7°40'13" W	108 ± 6	109.2 ± 1.4	191.4 ± 2.0	784 ± 19	10
052202 PC2	39°58'59" N 7°40'13" W	89 ± 6	77.4 ± 0.8	98.4 ± 0.9	727 ± 10	10
052204 PC4	39°58'59" N 7°40'13" W	52 ± 3	52.3 ± 0.5	75.5 ± 0.7	715 ± 9	10
052207 PC8	39°38'29" N 7°41'56" W	63 ± 11	70.3 ± 2.0	108.6 ± 2.1	621 ± 33	20
052208 PC9	39°39'19" N 7°40'07" W	19 ± 6	27.6 ± 0.6	29.6 ± 0.6	902 ± 17	25
052231 VRU4	39°38'29" N 7°41'56" W	78 ± 9	74.5 ± 1.0	114.3 ± 1.2	583 ± 12	20
052246 VRU5	39°38'29" N 7°41'56" W	27 ± 4	23.1 ± 0.4	28.0 ± 0.5	843 ± 12	10
052247 ENXAR1	39°58'59" N 7°40'13" W	44 ± 4	48.7 ± 0.5	75.1 ± 0.7	765 ± 8	10

Table 1. Cont.

NLL and Field Codes	X-Y Coordinates	U-238 (Bq kg ⁻¹)	Ra-226 (Bq kg ⁻¹)	Th-232 (Bq kg ⁻¹)	K-40 (Bq kg ⁻¹)	Water Content (%)
052253 VRU3	39°38'29" N 7°41'56" W	69 ± 7	61.3 ± 0.8	96.3 ± 1.1	536 ± 10	10
062201 ENXAR2	39°58'59" N 7°40'13" W	64 ± 7	68.4 ± 0.9	92.0 ± 1.1	764 ± 14	10
062202 PARN1	39°38'11" N 7°41'35" W	25 ± 5	27.9 ± 0.5	21.6 ± 0.5	843 ± 14	10
062203 PARN2	39°38'11" N 7°41'35" W	18 ± 5	24.9 ± 0.5	27.1 ± 0.5	995 ± 12	10

Table 2. Summary of the luminescence ages obtained from sediment samples from the study area. All ages were obtained by using a post IRIR₂₉₀ protocol (K-feldspar), in the Nordic Laboratory for Luminescence Dating (NLL). For samples having natural pIRIR₂₉₀ signals >86% of the saturation level of the dose response curves, a minimum age is given based on the 2*D₀ value. Previous IR₅₀ age estimates, including fading correction, are also shown [26].

NLL and Field Code	Sampled Site	Terrace Unit	Depth (cm)	IR ₅₀ , with Fading Corr. Age (ka)	pIRIR ₂₉₀ Age (ka)	pIRIR ₂₉₀ 2*D ₀ (Gy)	pIRIR ₂₉₀ D _e (Gy)	pIRIR ₂₉₀ Aliquots (n)	Dose Rate (Gy/ka)
052201 PC1	Foz de Enxarrique	T6, base middle part	550	38.5 ± 1.5	44 ± 3		350 ± 14	12	7.94 ± 0.32
052202 PC2	Foz de Enxarrique	T6, lower middle part	530	34.8 ± 1.3	43 ± 4		251 ± 21	9	5.83 ± 0.22
052204 PC4	Foz de Enxarrique	T5, middle part	150	136 ± 10	135 ± 9		683 ± 34	12	5.05 ± 0.18
052207 PC8	Vilas Ruivas	T5, middle part	400	105 ± 8	99 ± 7		507 ± 28	12	5.10 ± 0.19
052208 PC9	Rodense Bolaria	T4, lower part	200	277 ± 17	>220	>835 ± 51		6	3.95 ± 0.13
052231 VRU4	Vilas Ruivas	T5, upper part	400		71 ± 4		367 ± 17	9	5.18 ± 0.18
052246 VRU5	Vilas Ruivas	T4, lower part	300	277 ± 17	>220	>863 ± 13		6	4.19 ± 0.15
052247 ENXAR1	Foz de Enxarrique	T5, lower part	200	125 ± 7	145 ± 10		741 ± 40	12	5.11 ± 0.19
052253 VRU3	Vilas Ruivas	T5, middle part	400	113 ± 6	117 ± 7		587 ± 27	6	5.02 ± 0.19
062201 ENXAR2	Foz de Enxarrique	T6, topmost part	90	31.6 ± 1.3	37 ± 2		212 ± 6	6	5.73 ± 0.22
062202 PARN1	Pegos do Tejo-2 (Arneiro)	T4, lower middle part	400	209 ± 11	>190	>767 ± 27		9	4.14 ± 0.15
062203 PARN2	Pegos do Tejo-2 (Arneiro)	T4, lower top part	300	129 ± 11	>160	>743 ± 31		8	4.62 ± 0.17

Two of the four samples collected from T4 were collected from the lower gravel (052208 and 052246) and provided age estimates of c. 280 ka by IRSL and minimum ages of >220 ka by pIRIR. Samples 062202 and 062203 were collected from the base and middle of the T4 upper division which mainly consists of soft sandstones, and gave underestimated ages of 209 ± 11 ka and 129 ± 11 ka by IRSL and minimum ages of >190 ka and >160 ka by pIRIR, respectively. Sample 062203 was collected below the Middle Palaeolithic site of Pegos do Tejo-2, which is located c. 1 m below the T4 surface. As the uppermost deposits of T4 were recently dated at 155 ka ([28] (Cunha et al., 2017)) and sample 062203 provided a minimum age of 190 ka by pIRIR, it is very probable that the Middle Palaeolithic in the region had started by 200–170 ka.

From T5, which is overlapped by T6 at the Foz do Enxarrique site, ages of 145 ± 10 ka (at the terrace base) and 135 ± 9 ka (1.5 m below the terrace surface) were obtained by pIRIR dating. Samples collected from the T5 sequence at Vilas Ruivas were also dated, giving ages of 117 ± 7 ka, 99 ± 7 ka and 71 ± 4 ka by pIRIR.

From the T6 upper unit at Foz do Enxarrique, pIRIR dating provided the following three ages: 44 ± 3 ka, sample 052201 collected from the archaeological and fossiliferous bed (at a depth of 5.50–5.40 m); 43 ± 4 ka, sample 052202 collected from the micaceous fine sands located 20 cm higher (5.30–5.20 m); 37 ± 2 ka, sample 062201 collected c. 90 cm below the terrace surface (0.93–0.89) m. Previously, the archaeological bed was dated by Uranium series on equid and bovid teeth, providing an average age of 33.6 ± 5 ka ([48] (Raposo, 1995)), and by fading-corrected IRSL, giving an age of 38.5 ± 1.6 ka ([26] (Cunha et al., 2008)). It appears that both the U-series and conventional IRSL ages are underestimates, compared with the pIRIR ages. As previously noted, the IRSL dating used a correction for the anomalous fading effect which is not fully appropriate, leading to age underestimation. It should also be noted that U-series on teeth can easily be impaired as a result of the uptake of young uranium. The pIRIR protocol constitutes the best approach to date the type of material in consideration and should be considered to provide the best estimates for burial ages and for dating the associated lithic industries.

4.3. Sediment Characterization of T6

4.3.1. Mineral Composition

The sand and silt fractions of the T6 upper unit mainly comprise detrital grains of quartz (predominant), K-feldspar, plagioclase and muscovite, locally cemented by calcite. SEM and EDS analysis of 17 selected carbonate concretions also confirmed that these consist of calcite (micrite) developed in detrital silt–fine sand consisting of quartz (predominant), microcline, plagioclase and mica grains.

Exoscopy (SEM) (Figures 6 and 7) document well preserved microcline and quartz grains. The quartz grains are sub-angular and show conchoidal fractures, but with no evidences of abrasion or dissolution. Biotite grains show some dissolution features.

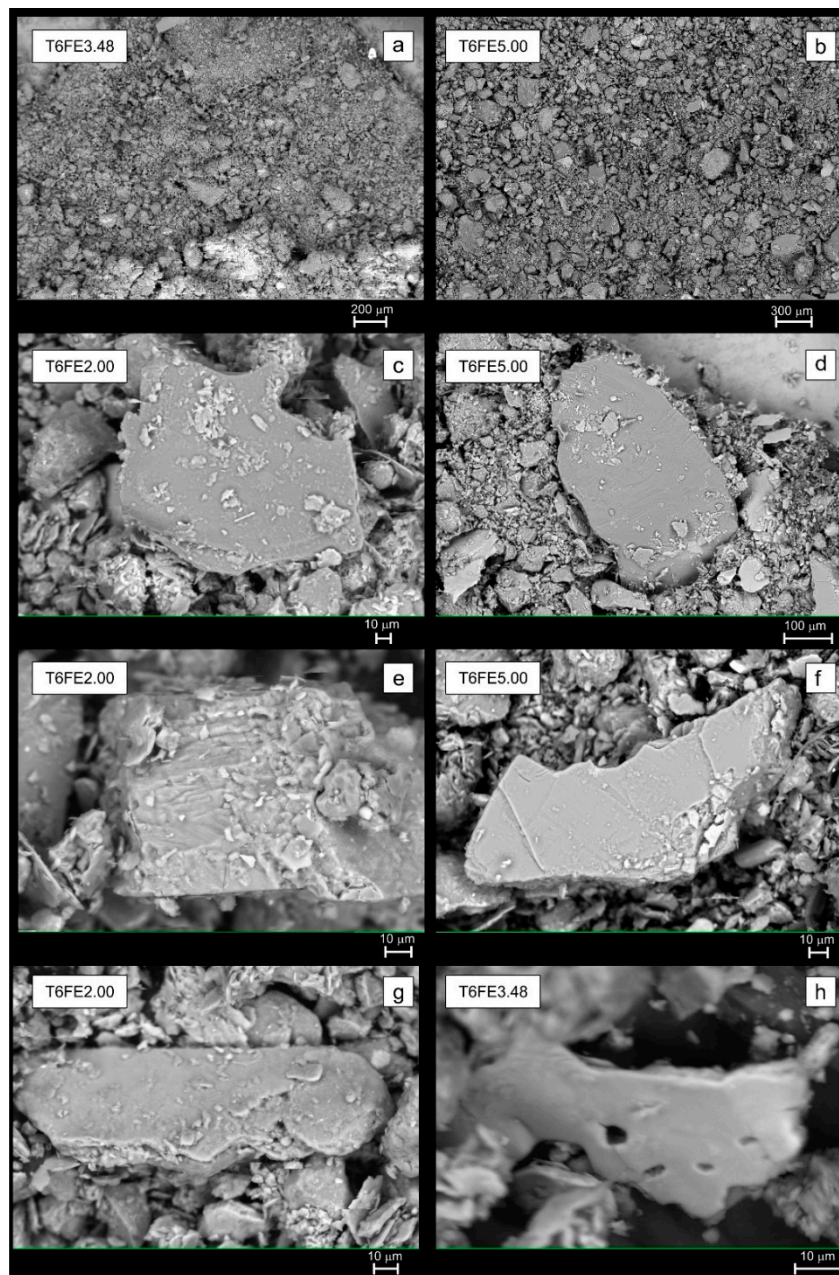


Figure 6. Back-scattered Scanning Electron Microscopy (SEM) photographs of samples from the T6 profile at Foz do Enxarrique. (a,b) poorly-sorted detrital material; (c,d) sub-angular quartz grain with conchoidal fractures and smoothed surfaces; (e,f) well preserved K-feldspar (microcline); and (g,h) mica grains, mainly biotite, with dissolution features.

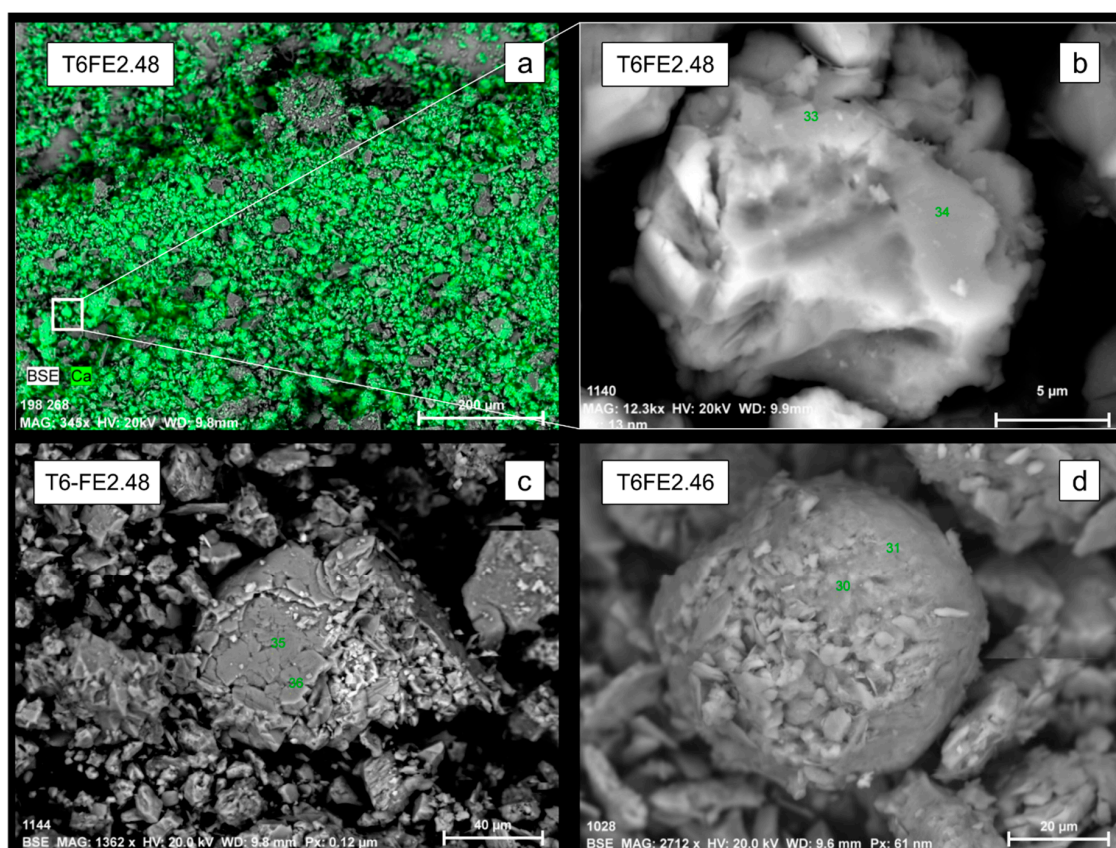


Figure 7. SEM photographs of samples T6FE2.46 and T6FE2.48. (a) compositional mapping showing the widespread distribution of calcium; (b,c) calcium particles and (d) nodules with size varying from 5 to 40 μm.

The mineralogical composition of the <2 μm fraction (Table 3) of 8 samples collected from the T6 upper unit does not indicate any vertical change and consists of smectite 35–52%, illite 22–35%, kaolinite 20–31% and vermiculite 17% (only present in sample T6FE 3.46–3.50). For comparison, two samples from T5 were also studied and contained smectite 53–54%, illite 21–29% and kaolinite 18–25%. Thus both terraces have a similar clay-mineral association, although T6 has less smectite. The modern sample also has vermiculite and chlorite.

Table 3. Mineralogical composition of the <2 μm fraction of samples collected from the T5, T6 upper unit and modern river bed of the Enxarrique stream.

Sample Code	Smectite (%)	Vermiculite (%)	Kaolinite (%)	Illite (%)	Chlorite (%)	Clay Mineral Association
T5FE0.15–0.23	54	0	25	21	0	Ski
T5FE0.92–1.00	53	0	18	29	0	Sik
T6FE0.70–0.74	48	0	26	26	0	Ski
T6FE1.13–1.17	52	0	23	25	0	Sik
T6FE1.97–2.02	41	0	27	32	0	Sik
T6FE2.88–2.92	47	0	31	22	0	Ski
T6FE3.46–3.50	35	16	25	24	0	Ski v
T6FE4.10–4.14	42	0	24	34	0	Sik
T6FE4.49–4.52	46	0	24	30	0	Sik
T6FE4.98–5.02	45	0	20	35	0	Sik
FE modern	17	14	22	35	12	Iks v c

4.3.2. Grain-Size Analysis

The sediment samples collected from the upper unit of T6 and analyzed by laser granulometry provided the results presented in Figure 4 and Supplementary Material. This unit is clearly dominated by coarse silt, but sampling at the 1 cm scale has documented significant grain-size oscillations as well as major grain size cycles.

From the 0.05–0.30 m depth, an organic dull yellowish to brown soil (10YR 5/3 and 10YR 4/6) has an average mean grain size of 41 μm . The samples are very poorly sorted (4.60) with very fine skewed (-0.72) distributions. In average, the sediment comprises 49% sand, 41% silt and 10% clay.

For the 0.31–5.00 m depth, the average grain-size data shows a mean grain size of 40.55 μm (very coarse silt), a standard deviation of 5.57 (very poorly sorted), fine skewed (-1.09), leptokurtic and bimodal distributions in the silt fraction (6–20 μm and 40–60 μm) (Figure 8). In average, the sediment comprises 44% sand, 45% silt and 9% clay. The range of mean grain size is 11–110 μm ; all main fractions change significantly: 6–72% sand; 25–78% silt; 3–20% clay. The following intervals can be differentiated to a depth of 5.00 m:

- For the 0.31–4.32 m depth, the samples have a yellowish to bright yellowish brown color, (10YR 5/3, 10YR 5/6, 10YR 5/8 and 10YR 6/8). The mean grain-size is c. 37 μm and is usually very coarse-grained silt. The average grain-size fractions consist of 40% sand, 49% silt and 10% clay. Some thin levels have calcium carbonate concretions reaching 1.5 cm of diameter (e.g., T6FE0.88; T6FE 0.95). There are some layers (e.g., at 1.15–1.20 m and 2.39–2.58 m depth) with much more silt (e.g., 76%; 68%) than sand.

- For the 4.33–5.00 m depth, the sediment is increasingly coarser, with a mean grain-size between 32 and 110 μm . In average, the sediment consists of 57% sand, 36% silt and 7% clay. Between depths of 4.73 and 4.82 m, rolled calcium carbonate concretions occur.

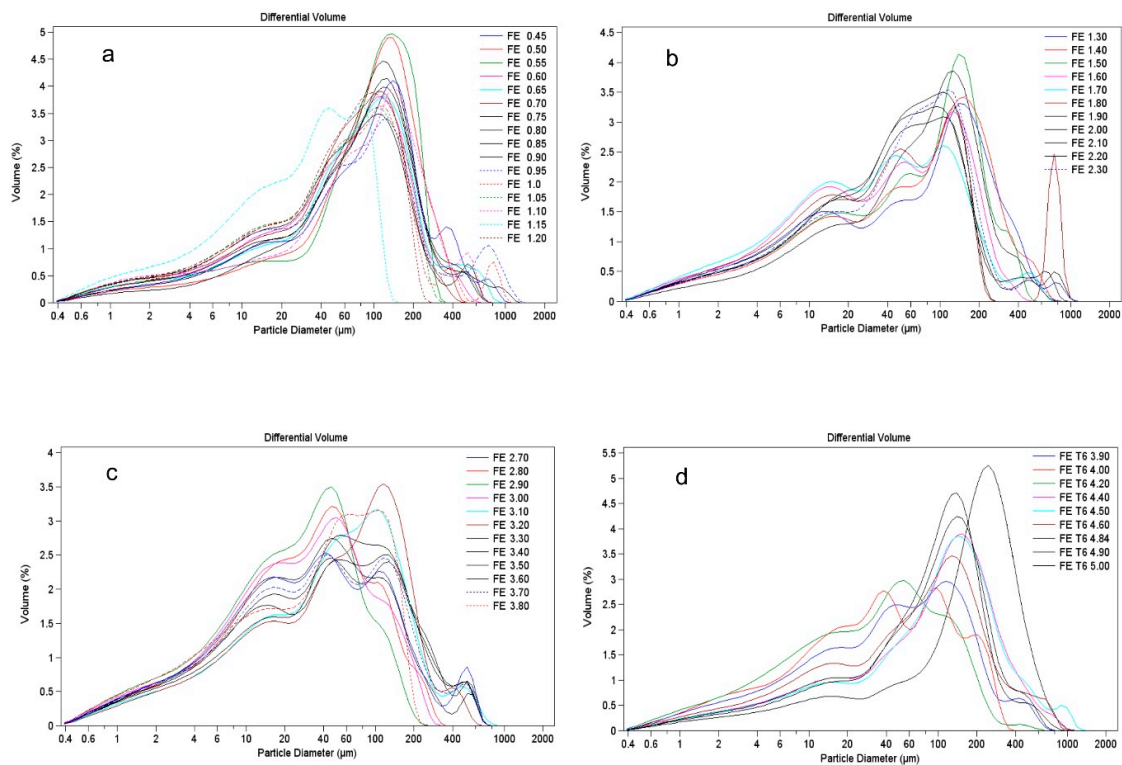


Figure 8. Grain size distributions of selected samples: (a) 0.45–1.20 m depth range; (b) 1.30–2.30 m depth range; (c) 2.70–3.80 depth range; (d) 3.90–5.00 m depth range.

4.3.3. Rock Magnetism

Magnetic Susceptibility

Mass specific magnetic susceptibility of samples from the Foz do Enxarrique T6 profile varies from c. 8×10^{-8} m³/kg to c. 6×10^{-7} m³/kg (Table S1—Supplementary Material; Figures 4, 9 and 10). These values are comparable with those of suspended sediments from other fluvial systems, such as the Jackmoor Brook catchment in South West England [49]. The lowest values of magnetic susceptibility (c. 7×10^{-8} m³/kg) are found at the base of the profile, from c. 5.00 up to 4.58 m, and corresponding to sand-rich sediment (Figure 4). From 4.57 up to 4.32 m, there are some dispersed quartzite pebbles; magnetic susceptibility increases and exhibits saw-tooth oscillations from c. 1.2×10^{-8} to 4.1×10^{-8} m³/kg. Between 4.32 and 0.40 m, magnetic susceptibility shows short-term and discrete cyclical oscillations from 1.4×10^{-7} to c. 3.7×10^{-7} m³/kg and gradually increases up to c. $5.5\text{--}8 \times 10^{-8}$ m³/kg in the uppermost 0.40 m.

Magnetic susceptibility is primarily controlled by lithological changes, but can also reflect pedogenic and/or post-depositional weathering driven by environmental and climatic forcing in the case of continental sediments [50]. Quartz is diamagnetic (negative and very low magnetic susceptibility), explaining the very low values of magnetic susceptibility observed at the base of the profile (Figure 4). Phyllosilicates, including clays, are paramagnetic (positive and weak magnetic susceptibility), giving significant higher values of magnetic susceptibility in the silt interval from 4.32 m to 0.40 m. The short-term cyclical variations observed in this part of the profile do not seem to be controlled by the lithology, which is very homogenous in the field, but may reflect changes in the magnetic mineralogy (ex. proportion of magnetite and hematite), including magnetic enhancement by weathering and/or pedogenic processes. The saw-tooth oscillation observed from 4.57 m to 4.32 m probably reflects the mixture of gravel with different origin and composition. In contrast, the increase of magnetic susceptibility in the topsoil horizon, which corresponds in the field to a black sediment, rich in organic material, probably reflects magnetic enhancement resulting from burning, pedogenic processes and/or anthropogenic pollution [51–53].

Frequency-Dependence Magnetic Susceptibility

Frequency-dependence magnetic susceptibility varies between 4 and 10 along the entire profile, indicating a significant contribution from superparamagnetic particles. These superparamagnetic particles are generally ultra-fine magnetite and/maghemite produced during pedogenic processes, as a by-product of the metabolism of iron-reducing bacteria [54,55]. The presence of pedogenic magnetic particles in the T6 profile agrees with the ubiquitous occurrence of rhizoliths (root moulds and concretions) observed in the field. However, these pedogenic particles can also have a detrital origin, from the incorporation of soil sediments or clays.

Isothermal Remanent Magnetization Curves

Isothermal Remanent Magnetization (IRM) measurements were conducted on eight samples from the T6 profile in order to investigate the nature and origin of the ferromagnetic particles present in the sediment and their contribution in the short-term cyclical oscillations observed in the magnetic susceptibility curve. In addition, a sample of modern sediments was analyzed for comparison. Results are shown in Table 3 and Figure 9. After treatment of the raw data by the cumulative Log-Gaussian function [37], two main components are obtained in all samples. Component 1 has $B_{1/2}$ values of 21–24 mT and DP (dispersion parameter) of 0.25–0.30, corresponding to the coercivity range of detrital magnetite [56]. Magnetite contributes to 77–83% of the total remanence. Component 2 has $B_{1/2}$ values of 200–234 mT and DP of 0.50–0.55, typical of hematite [56]. Hematite contributes to 17–22% of the total remanence. Goethite has not been identified although the data are noisy above imparted fields of 1 T. The S-ratio varies between 0.86 and 0.92 and reflects the dominance of magnetite in the total remanence.

Except for the slight variations of the S-ratio, no significant changes in the magnetic mineralogy (coercivity and grain-size) was noted within the eight analyzed samples, nor with modern sediments (Figure 9). However, there is a clear correlation between magnetic susceptibility and saturation isothermal remnant magnetization (SIRM), suggesting that magnetic susceptibility is mostly controlled by the concentration of ferromagnetic iron oxides (magnetite and hematite) (Figure 10). In addition, samples having the lowest magnetic susceptibility values also have lower S-ratio (Table 4), suggesting that the short-term cyclical variations observed in the magnetic susceptibility curve reflect variation in the relative proportion of magnetite and hematite.

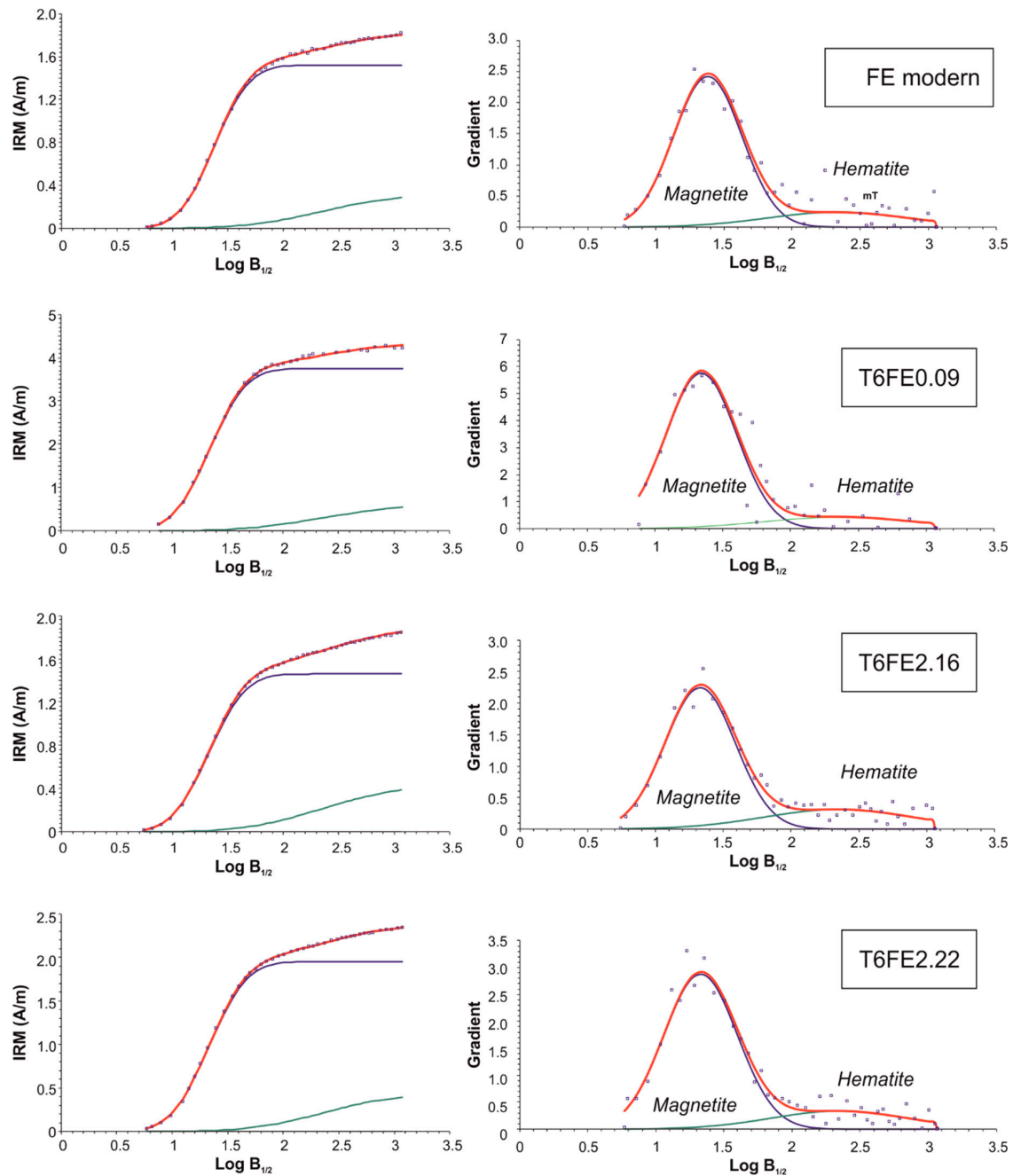


Figure 9. Isothermal Remnant Magnetization (IRM) curves treated by the log-Gaussian function, of representative samples from the upper unit of T6 (the sample depth is indicated by the sample reference) and present-day sediment from the Enxarrique stream (sample FE modern), all collected at the Foz do Enxarrique site.

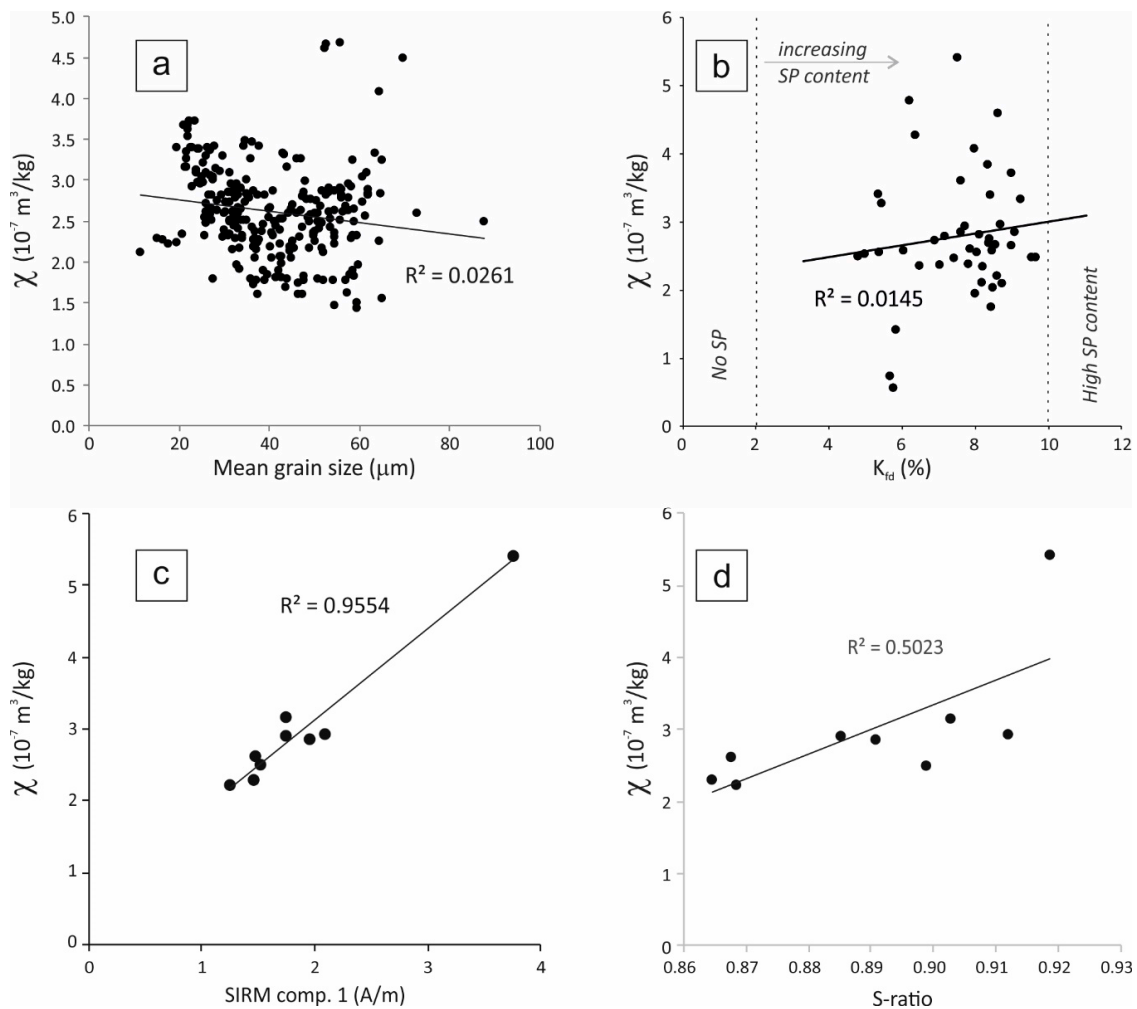


Figure 10. Correlations between mass specific magnetic susceptibility and (a) grain size, (b) frequency-dependent magnetic susceptibility and (c) Saturation Isothermal Remanent Magnetization of component 1 (i.e., magnetite content) and (d) S-ratio (relative proportion of magnetite and hematite). R² is the determinant factor.

Table 4. Rock magnetic parameters calculated from the analysis of the IRM curves (see Figure 9). The % column represents the percentage of the contribution of the magnetic phase; SIRM is the IRM at saturation is proportional to the concentration of the magnetic phase; B1/2 corresponds to the coercivity and DP is the dispersion parameter of the Gaussian curves.

Sample Code	Component 1 (Magnetite)				Component 2 (Hematite)				
	%	SIRM	B1/2	DP	%	SIRM	B1/2	DP	S-Ratio
FE modern	83.1	1.52	24.0	0.25	16.9	0.31	218.8	0.52	0.90
T6FE0.09	86.2	3.75	21.9	0.26	13.8	0.60	223.9	0.55	0.92
T6FE0.62	77.8	1.47	21.9	0.26	22.2	0.42	223.9	0.55	0.87
T6FE2.00	80.6	1.75	21.9	0.3	19.4	0.42	223.9	0.55	0.89
T6FE2.16	77.2	1.46	21.4	0.26	22.8	0.43	223.9	0.55	0.86
T6FE2.22	82.3	1.95	21.4	0.27	17.7	0.42	223.9	0.50	0.89
T6FE2.33	76.7	1.25	21.4	0.26	23.3	0.38	199.5	0.53	0.87
T6FE3.74	84.3	2.09	22.4	0.25	15.7	0.39	199.5	0.53	0.91
T6FE3.84	79.5	1.75	22.4	0.25	20.5	0.45	158.5	0.50	0.90

4.3.4. Phytolith Analysis

Phytoliths were identified in those carbonate concretions corresponding to samples with codes T6FE0.72, T6FE2.00, T6FE2.90, T6FE3.48 and T6FE4.12, but constituted fewer than 10 units per observed concretion, which limits their potential for environmental interpretation. The identified morphotypes are predominantly larger than 20 μm , of Bulliform and Cuneiform types (Figure 11) and rare Elongates and Trapeziforms. The Bulliform and Cuneiform types are usually produced by grasses undergoing hydric stress. The poor preservation of the studied phytoliths is probably due to the alkalinity of the concretions, although there is some evidence of aeolian abrasion.



Figure 11. Phytoliths of Bulliform and Cuneiform types, identified in carbonate concretions. Scale bar: 20 μm .

4.3.5. Palynology

From a general point of view, the prepared residues from both the T6 and T5 terraces are very poor in organic matter and pollen. A small number of highly degraded pollen grains were observed, of which some are indeterminable because of their damaged state. The small number of identified pollen grains and, in some cases, the sterility of the samples, precludes the construction of pollen diagrams. The results are presented in Table 5, organized by sample; taxa for each sample are divided into arboreal types, followed by shrubs and herbaceous and, finally, indeterminate pollen grains.

Table 5. Palynology of the T6 and T5 terrace deposits, from the stratigraphic sections at Foz do Enxarrique site.

Sample Code	Taxa	Count
Basal layer (archaeological strata) of the T6 upper unit		
FE/15 0.25–0.30	Indeterminate	1
FE/15 0.35–0.40	Chenopodiaceae	2
	Indeterminate	4
FE/15 0.45–0.50	Indeterminate	2
Upper part of the T6 upper unit (silty sands and sandy silts)		
T6FE0.70–0.74	<i>Pinus</i> sp.	4
	Ericaceae	2
	Poaceae	2
	<i>Artemisia</i>	1
	Chenopodiaceae	2
	Indeterminable	9

Table 5. Cont.

Sample Code	Taxa	Count
Upper part of the T6 upper unit (silty sands and sandy silts)		
T6FE1.13–1.17	<i>Pinus</i> sp.	1
	Poaceae	2
	Indeterminate	10
T6FE1.97–2.02	<i>Pinus</i> sp.	1
	<i>Asteraceae tubuliflora</i>	1
	Indeterminate	6
T6FE2.88–2.92	Indeterminate	1
T6FE3.46–3.50	Indeterminate	3
T6FE4.10–4.14	Indeterminate	1
T6FE4.49–4.52	Indeterminate	1
T6FE4.98–5.02	<i>Pinus</i> sp.	1
	Indeterminate	1
T5 lower part (sandy silts)		
T5FE0.15–0.23	Indeterminate e	1
T5FE0.92–1.00	<i>Pinus</i> sp.	1
	Indeterminate	2

The two samples from the lower part of the T5 sequence from outcrops at the Foz do Enxarrique site (T5FE015–0.23 and T5FE0.92–1.00) only allowed the identification of a pollen grain of *Pinus* sp. For the three samples collected from the basal layer (archaeological strata) of the T6 upper member only Chenopodiaceae could be identified. In the samples collected in the upper part of T6, the few taxa identified indicate the presence of *Pinus* sp., the only tree species, Ericaceae (shrubs) and, in the herbaceous group, Poaceae, *Artimisia*, Chenopodiaceae and *Asteraceae tubuliflora*. In conclusion, the results obtained from the palynological study of the T6 and T5, from oxidized sediments, revealed very few palynomorphs and do not allow any palaeoenvironmental interpretation.

4.3.6. Geochemical Analyses

The results of geochemical analyses performed with the Thermal Scientific Analyzer Nikon XL3t spectrometer, on samples collected from the upper unit of T6, indicate that Ca has high values on the calcium carbonate concretions/rizoliths and very low values on uncemented siliciclastic sediment (coarse silt to fine sand) (Appendix A, Figure A1).

4.4. Palaeolithic Sites and Fauna Associated

No evidence has been found to date of industries prior to the Acheulean in this area. However, considering the presence of Oldowan material at several sites in Iberia, some dating back to c. 1.4 Ma, this absence must be seen as a problem of archaeological visibility [57].

The oldest archaeological evidence in this region appears in the basal deposits of T4, which are dated as older than 280 ka and perhaps as old as c. 340 ka [26,28]. A large Acheulean quartzite assemblage, with handaxes, cleavers, very large flakes and respective cores, was recovered from Monte do Famaco (Vila Velha de Ródão), in a colluvium resulting from the erosion of basal T4 deposits [58]. Test pits were excavated at this site and a large assemblage was also collected from the surface, but no thorough excavation was undertaken, nor has the assemblage been published in detail. Other evidence of Acheulean (e.g., identification of single or small numbers of handaxes and cleavers, sometimes

along with quartzite flakes) has been reported from T4 deposits at Vilas Ruivas (Arneiro), but also at the surface of Pegos do Tejo-1, Monte das Nove Oliveiras, Monte do Arneiro and Monte da Cabeça Gorda; all these sites at Arneiro are still to be excavated [59,60].

The earliest Mousterian (Middle Paleolithic) industries occur on both sides of the Tejo in the uppermost deposits of T4. At Pegos do Tejo-2 (probably dating from c. 200–170 ka), the identification of a ring of cobbles was interpreted as a possible hearth (fire pit). These occur along with Levallois, discoidal, opportunistic and bipolar cores, flakes (often thick), denticulates, notches and sidescrapers [61,62]. A similar age (c. 165–155 ka) was attributed to Cobrinhos (Vila Velha de Ródão), a dense lithic assemblage spread over 1300 m² and dominated by Levallois, discoidal, radial and opportunistic cores and Levallois and *Kombewa* flakes (and also some points and blades), pseudo-Levallois points, sidescrapers, denticulates and notches [22].

At Monte da Revelada (Vila Velha de Ródão), also at the top of T4, the lowest archaeological context has discoidal and Levallois cores, flakes with dihedral and faceted platforms, along with radial dorsal patterns, including some Levallois flakes and pseudo-Levallois points that can be associated with a Mousterian occupation. These artefacts occur along with oval stone features that that again may correspond to hearths. At the nearby site of Alto da Revelada, Mousterian artefacts occur scattered on the surface, on the Cabeço do Infante Formation (Paleogene), in the western area where it has not been covered by aeolian sands [63].

In the T5 deposits at Vilas Ruivas (Arneiro), now dated to c. 117–71 ka, it was again possible to recognize hearths, windshields and post-holes [59,60], associated with a small but well-preserved Mousterian assemblage. This was composed of Levallois, discoidal and centripetal cores, Levallois flakes, pseudo-Levallois points, some blades and points, denticulates, notches and sidescrapers, mostly quartzite, but without faunal remains.

At Azinhal (Arneiro), archaeological evidence located at an alluvial deposit dated to c. 61 ka and connected with T6 terrace, corresponds with a lithic assemblage dominated by quartzite (62%), quartz (36%) and some flint (2%), with discoidal, centripetal and opportunistic cores, Levallois flakes and blades, choppers, perforators, burins, denticulates and handaxes, suggesting some mixture with both Acheulean and Upper Paleolithic [61,62].

At Tapada do Montinho (Arneiro), a site in an alluvial fan unit dated to c. 51 ka and connected with T6, the lithic assemblage is composed of quartzite (84%), quartz (10%) and flint (5%) and comprises *Kombewa*, Levallois, and discoidal cores and Levallois flakes along with notches [61,62].

At the Foz do Enxarrique site, several archaeological campaigns were undertaken between 1982 and 2001. A single archaeological level was identified, at the base of the T6 upper unit, with a diverse Pleistocene faunal assemblage associated with a rich Mousterian industry represented by more than 10,000 artefacts [48,64]. Among them are Levallois, discoidal and centripetal cores, Levallois flakes and pseudo-Levallois points, plus blades and points, denticulates, notches and sidescrapers, most of them produced from quartzite (c. 66%), quartz (c. 25%) and flint (c. 9%). A complete sequence of debitage is present. The exploitation of raw materials was interpreted as resulting from local and opportunistic procurement [48].

The Foz do Enxarrique faunal assemblage from the campaigns carried out between 1982 and 1999, a total of 785 bone specimens, was studied by Brugal and consists of red deer (*Cervus elaphus*—54.8%), horse (*Equus caballus*—36.5%), aurochs (*Bos primigenius*—2.2%), elephant (1.2%), rhinoceros (0.5%), rabbit (4.2%), and a very few carnivores such as fox (0.5%), hyena (0.2%) and lynx (0.2%) [65–68]. The fauna collected during later campaigns (2000 and 2001) has the same characteristics: a clear predominance of deer, horse and aurochs; the predominance of these herbivores and the weak occurrence of carnivores points to an anthropogenic accumulation [69]. This seems to be reinforced by the distribution of the anatomical units of the skeleton identified from the most commonly represented species (*Cervus* and *Equus*). The cranial specimen is the most represented (47.3% for the deer and 75.3% for equidae), the axial and appendicular skeleton representing only 52.7% and 24.7%, respectively [66]. This suggested the idea that the site served as a hunting zone, because the edible parts (associated

to the appendicular and axial skeleton) have been removed. Such interpretation is more difficult for the megafauna assemblage as, for instance, in the case of the elephant remains (classified as *Elephas antiquus* (= *Paleoloxodon antiquus*)) that are represented by a lamella of a superior molar and four bone fragments [66–68]. Worthy of note is the occurrence of birds, fish and mollusc remains [66]; however, in a subsequent study no bird bones have been identified [69]. Amongst the studied remains, just over 50% are small fragments of unidentified bones; there are 42% of identified remains, which represents a high rate compared to other Paleolithic sites, where the fauna remains appear very fragmented (10 to 20% of total remains: TNR) [66]. About 13 specimens were identified with marks from the action of carnivores and 15 with marks from human butchery (nine with cutmarks and six with evidence of burning) [66]. Results from use–wear study on the lithic assemblage performed on 110 quartzite artefacts showed a dominance of wear traces associated to butchering, cutting of soft-animal tissue and scraping on bone activities [70]. Based on this, the authors conclude that the site was primarily a hunting zone, in which the animals were killed, quartered and then mainly taken to other places.

The Carregueira Formation (the cover unit of aeolian sands) contains Late Palaeolithic to Neolithic industries. At Monte da Revelada, the upper bed is composed of aeolian sands, disturbed by ploughing, and contains a mixture of Epipaleolithic and Neolithic material. A similar context, but here with backed bladelets, was found within the aeolian sands covering the eastern area of Alto da Revelada. At Vilas Ruivas, the aeolian unit, again disturbed by ploughing, has a Late Upper Palaeolithic or Epipaleolithic industry, in which flint occurs in greater quantity and the lithic assemblage has prismatic cores, blades and bladelets, small flakes, burins and endscrapers. Therefore, it is possible that the MIS 2 aeolian sands of the Carregueira Formation may preserve the first modern human occupations in the region.

5. Discussion

Regarding the environmental interpretation of the T6 record in the study area, the lower boulder–pebble gravel, 0.4 m thick and overlying a strath cut in metamorphic basement, corresponds to the coarse river-bed sedimentation near the margin of the energetic Tejo palaeochannel, probably during the interval c. 60–45 ka (MIS 3). No lithic artefacts or fossils, which could have helped in the interpretation, were found in this bed.

The T6 upper unit, mainly consisting of fine to very fine sands, grading upwards to coarse silt, is attributed overbank sedimentation. The detailed environmental interpretation of the various stratigraphic subunits is discussed in the following paragraphs.

The c. 20 cm lower bed (at 5.60–5.40 m depth), comprising Mousterian artefacts and fossil bones in a matrix of gravelly micaceous fine sands, is interpreted as overbank deposits close to the channel margin that also record hominin activities of hunting and butchery [48,64,66,70]. During this period, the Tejo channel moved laterally towards the west, preserving this record of human occupation. Thus, this confined place at the confluence of the Enxarrique and Açafal streams was used by animals for drinking and they were easily hunted. As this thin layer, now dated to 44 ± 3 ka, represents the last regional evidence of Mousterian industries and the megafauna, it may correspond to a cold and dry period that negatively impacted the animals and the Neanderthals. It is possible the Neanderthals relied heavily on some specific biotic resource that may have been reduced during cold climatic conditions, so that they faced difficulties in adapting. The remaining Neanderthals could have been induced to move toward the better climate conditions of SW Iberia and were later absorbed into modern human populations. Also relevant to this discussion is the fact that the ages of the stratigraphic levels with the youngest Mousterian industries in westernmost Iberia are progressively younger toward the SSW: the Cantabrian region, c. 48–45 ka [71]; central Portugal, c. 44–34 ka (e.g., Foz do Enxarrique, c. 44 ka; Almonda, c. 32 ka; Mira Nascente, c. 42–40 ka; Gruta da Figueira Brava, c. 34 ka) [58,72–75]; Murcia, 37 ka [11]; Gibraltar, between c. 33 and 24 ka [9].

The sediments of the 5.40–4.55 m depth interval within T6, consisting of micaceous fine sands with some interbedded thin gravel stringers, are also attributed to fluvial overbank deposition close to

the channel margin. No fossils or artefacts were found here or in the upper deposits of T6. The onset of a new sedimentation phase (overbank fine-grained sediments) without artefacts is not necessarily evidence for cultural breakdown. However, in other areas of the Lower Tejo where T6 is preserved, no Mousterian artefacts were found in younger stratigraphic levels.

Regarding the T6 upper unit, the coarse silts from 4.55 cm depth to the surface are attributed to overbank sedimentation, but some characteristics point to the possibility of short-distance transport by wind, namely the lack of lamination and of erosion surfaces, the absence of dispersed coarser grains, the low clay content, a mean grain size in the coarse silt range, the fine skewed distributions and evidence of aeolian abrasion provided by phytolith analysis. The literature shows grain-size-distribution curves of loess deposits to be very similar to these silty T6FE deposits (e.g., [76–80]). Possible short-distance aeolian transport of exposed overbank fines could have been promoted by strong winds coming from the west and penetrating through the Ródão gorge (Figure 1). However, if there had been significant aeolian transport, the resultant sediments should also cover higher terrace levels, and this is not evidenced by field observation.

Sediment magnetic properties have been widely applied to fluvial sediments and loess and may provide useful information about fluvial activity, climate and environmental changes, as well as pedogenesis [50,51,81–83]. In fluvial sediments from Beijing, for example, high magnetic susceptibility values generally reflect warm-climate conditions, whereas lower values match colder periods [84]. In wind-blown sediments and buried soils from southern Siberia [81], colder high-wind periods that are associated with an absence of soil formation show low values of frequency-dependence of magnetic susceptibility, whereas higher values are observed in episodes with less wind. In the classic loess–palaeosol sequence of the central Chinese Loess Plateau, there is a striking correlation between magnetic susceptibility and grain size [85], which are good indicators of summer and winter monsoon intensity respectively [86,87]. In general, ferromagnetic crystals in soils derive from both primary (detrital) and secondary (enhanced) iron minerals. The latter are most often of stable single-domain size or less and associated with the clay fraction, whereas the former are usually associated with sand and coarse silt-size fractions [49]. Regarding the studied T6 sediments, no significant correlation ($R^2 = 0.0261$) is observed between sedimentary grain size and magnetic susceptibility, suggesting that the latter is not controlled by mineralogy (ex. paramagnetic clay and phyllosilicates versus diamagnetic quartz) (Figure 5). In contrast, a striking correlation between SIRM and magnetic susceptibility ($R^2 = 0.9554$ for magnetite; $R^2 = 0.769$ for hematite) indicates that magnetic susceptibility is dominantly controlled by the iron-oxide content, in the form of magnetite and hematite (Figure 10), probably of a detrital origin. The proportion and contribution of magnetite and hematite in the bulk remanence is mostly similar in all samples, as illustrated by narrow S-ratio values of 0.86–0.92. In particular, the IRM curves of the T6 samples are very similar to those of modern sediments (Figure 9), suggesting a common source for the entire sedimentary profile during the last millennium. Superparamagnetic particles, generally interpreted as a product of pedogenic processes, are present in all samples and may have been formed in situ or transported from the surrounding soils. The presence of numerous rhizoliths observed in the field suggests that pedogenic magnetic particles may have precipitated in-situ, during soil development. However, the poor correlation ($R^2 = 0.0145$) between mass specific magnetic susceptibility and frequency-dependent magnetic susceptibility indicates that pedogenic processes alone cannot explain the short-term cyclical variations observed in the magnetic susceptibility curve of the T6 profile (Figure 4). Conversely, a slight but significant correlation ($R^2 = 0.5023$) between the S-ratio, i.e., the relative proportion of magnetite versus hematite, and magnetic susceptibility imply that the short-term cycles may correspond to changes in weathering regime and climate. More exactly, warmer/drier periods would enhance the oxidation of magnetite (or maghemite) and promote precipitation of hematite, and the reverse. Because the magnetic susceptibility of hematite is lower than magnetite, this provides a potential explanation for the cyclical oscillations observed in the magnetic susceptibility curve.

The 0.60–5.40 m depth interval contains c. 30 thin levels of calcium carbonate concretions and rizoliths intercalated in uncemented coarse silt. The characteristics of these levels, which have no evidence of any erosive surface and dip toward the palaeochannel, progressively increasing in thickness, point to a secondary origin for the carbonate concretions. A relatively stable surface and a certain amount of rainfall during the represented periods are indicated. The most probable source of calcium carbonate for these pedogenetic concretions is the dissolution of dolomitic and calcium carbonates that occur at the base of the Cabeço do Infante Formation (Paleogene), which crops out at a short distance from the site. Upstream sources of calcium carbonates are located at least at 200 km away (in the Madrid Cenozoic basin).

The aggradation of T5 (c. 140–70 ka) correlates with the very high sea levels of MIS 5, whereas the following period of river down-cutting (c. 70–60 ka) indicates to have been mainly determined by the low-sea-level conditions during MIS 4 and the aggradation of T6 (c. 60–32 ka) seems to correlate with the higher sea levels and high sediment supply coeval with MIS 3 [2,27,28]. During this interval (c. 140–32 ka) Iberia was influenced by several climatic (e.g., [88–92]) and oceanographic changes [93,94], registered in the North Atlantic region and in records from Greenland Ice Cores (e.g., [95,96]).

The results obtained from palynological study of the T6 and T5 deposits do not allow palaeoenvironmental interpretation. Regarding the interval represented by the T6 terrace, the palynological record of the MD95-2039 ocean core points to an open landscape with steppe vegetation and low values of tree pollen, suggesting a severely cold and dry climate, during 61–59 ka; during the interval 57–31 ka, there are fluctuations in the expansion and contraction of arboreal pollen and Ericaceae related to the alternation of warmer and humid conditions during the interstadials and the cold and dry stadial minima of the last glacial cycle [92]. In the Puente Pino sequence (Toledo, Spain), for the 42–34 ka interval, declining woodland and the increasing herbaceous pollen taxa are observed, related to adverse climate conditions of cold and dry character [97]. The palaeoenvironmental data provided by these two adjacent contexts support the possibility of an open landscape in the region of the study area and could explain the several levels with pedogenic calcium carbonate rizoliths and concretions in the T6 upper unit.

The mineralogical composition of the <2 µm fraction of the samples collected from T6 and T5 are similar, consisting of smectite, illite and kaolinite, although T6 has less smectite. Even if a significant part of the clay minerals could have been sourced from erosion of the local Paleogene and Miocene formations, very rich in smectite [23,25], this clay mineral association seems compatible with the regional climatic conditions during MIS 5–3 [91,92].

By 32 ka, the climate had changed to cold and dry conditions and aeolian deposition dominated the valley landscape, preserving Upper Palaeolithic industries.

6. Conclusions

Updated ages from the three Lower Tejo terrace sequences, containing Mousterian industries, were obtained by pIRIR, as follows:

(i) OSL dating of the oldest Mousterian industry, stratigraphically situated in the uppermost T4 deposits, suggests a probable age of c. 200–170 ka for the arrival of the Neanderthals in this region, probably by way of the Tejo River valley from central Iberia;

(ii) T5 dates from c. 140 ka at the base and 70 ka at the top;

(iii) T6 dates from c. 60 ka at the base and c. 35 ka near the top;

(iv) The new date of 44 ± 3 ka for a level located at the base of the T6 upper unit records the last regional occurrence of a Mousterian industry and of the megafauna.

The T6 upper unit (so far without Mousterian or Early Upper Palaeolithic industries), consists of fine sands to coarse silts interpreted as overbank sediments. It has a large number of intercalated thin levels of carbonate concretions and rizoliths, suggesting episodic evaporation and development of paleosols in a seasonal dry period, in agreement with the occurrence of phytoliths.

Supplementary Materials: The following is available online at <http://www.mdpi.com/2571-550X/2/1/3/s1>. Table S1—Grain-size statistical parameters and mass specific magnetic susceptibility of samples collected from of the T6 upper unit at Foz do Enxarrique site.

Author Contributions: Conceptualization, P.P.P.; Methodology, P.P.C. and E.F.; Validation, P.P.C., J.-P.B., M.P.G., E.F., P.Y. and R.M.; Formal Analysis, J.-P.B., A.S.M., M.P.G., E.F., C.F., P.Y., J.C.S. and R.M.; Investigation, P.P.C., A.A.M., J.-P.B., A.S.M., M.P.G., E.F., T.P., S.F., C.F., P.Y., J.C.S. and R.M.; Writing-Original Draft Preparation, P.P.C., A.M., M.P.G., E.F., T.P., S.F., C.F., D.R.B.; Writing-Review & Editing, P.P.C., A.A.M., J.-P.B., E.F., T.P., S.F., C.F., D.R.B.; Visualization, A.A.M., P.P.C., M.P.G., E.F., P.Y., R.M.; Supervision, P.P.C.

Funding: This research was part funded by the Fundação para a Ciência e a Tecnologia, through projects, UID/MAR/04292/2013—MARE (PPC, MPG, YP and RM), UID/GEO/04683/2013—ICT (SF and CF), UID/GEO/04683/2013—ICT (AAM) and IF/01075/2013 (TP). MPG has the FCT PhD grant SFRH/BD/116038/2016.

Acknowledgments: Thanks to Ana Bárbara Costa, Johannes Remhof, José Erbolato Filho, Alexandre Cabral and Paulo Pedrosa for assistance during fieldwork and at the Sedimentology Laboratory. Lídia Catarino is thanked for assistance during the use of the Thermal Scientific Analyzer Nikon XL3t spectrometer. Luis Raposo and Nelson Almeida provided very constructive comments regarding the Palaeolithic of the area. Thanks to the reviewers and editor for manuscript improvements.

Conflicts of Interest: The authors declare no conflict of interest. The funders had no role in the design of the study; in the collection, analyses, or interpretation of data; in the writing of the manuscript, or in the decision to publish the results.

Appendix A

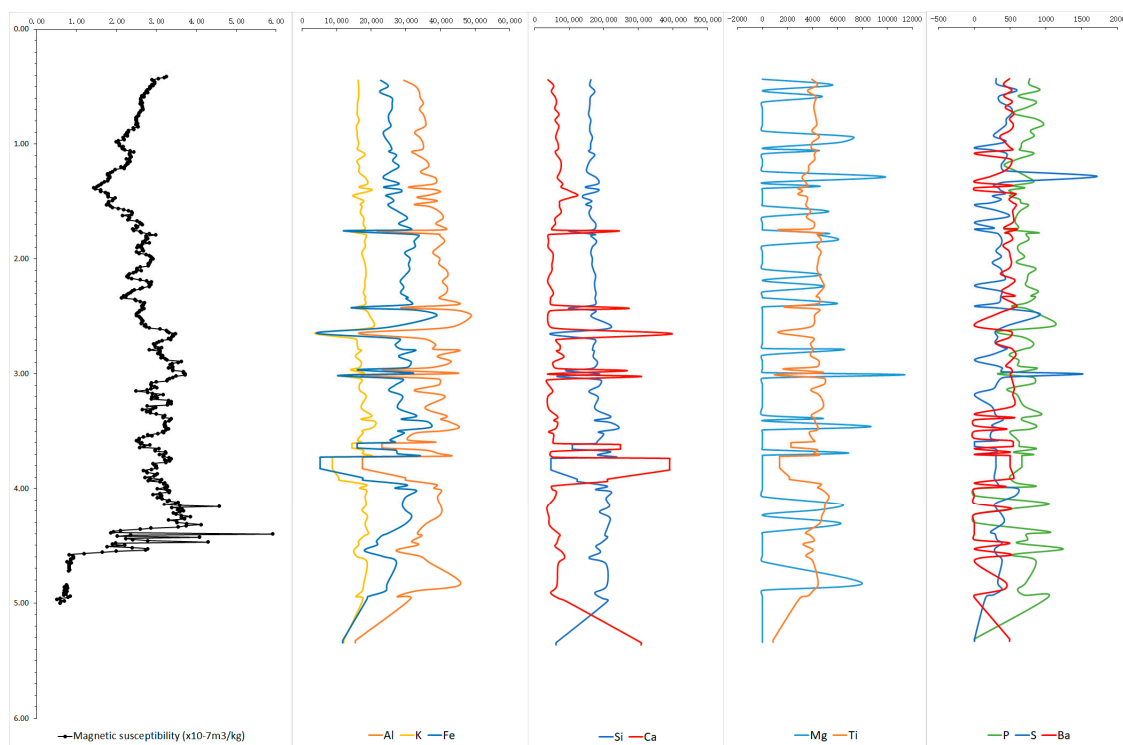


Figure A1. Comparison between the mass specific magnetic susceptibility results and the results of geochemical analyses performed with a X-ray fluorescence spectrometer (Al, K, Fe; Si, Ca; P, S, Ba, Mg and Ti), on samples collected from the upper unit of T6 at Foz do Enxarrique (sample depth in meters).

References

1. Cunha, P.P.; Martins, A.A.; Daveau, S.; Friend, P.F. Tectonic control of the Tejo river fluvial incision during the late Cenozoic, in Ródão—Central Portugal (Atlantic Iberian border). *Geomorphology* **2005**, *64*, 271–298. [[CrossRef](#)]

2. Cunha, P.P.; Almeida, N.A.C.; Aubry, T.; Martins, A.A.; Murray, A.S.; Buylaert, J.-P.; Sohbati, R.; Raposo, L.; Rocha, L. Records of human occupation from Pleistocene river terrace and aeolian sediments in the Arneiro depression (Lower Tejo River, central eastern Portugal). *Geomorphology* **2012**, *165–166*, 78–90. [[CrossRef](#)]
3. Zilhão, J. Le passage du Paléolithique moyen/Paléolithique supérieur dans le Portugal. In *El Origin Del Hombre Moderno En El Suroeste de Europ*; UNED: Madrid, Spain, 1993; pp. 127–146.
4. Zilhão, J. The Ebro Frontier: A Model for the Late Extinction of Iberian Neanderthals. In *Neanderthals on the Edge: 150th Anniversary Conference of the Forbes' Quarry Discovery, Gibraltar*; Oxbow Books Limited: Oxford, UK, 2000; pp. 111–121.
5. Zilhão, J. Chronostratigraphy of the Middle-to-Upper Paleolithic Transition in the Iberian Peninsula. *Pyrenae* **2006**, *37*, 7–84. [[CrossRef](#)]
6. Zilhão, J. The Ebro frontier revisited. In *The Mediterranean from 50,000 to 25,000 BP: Turning Points and New Directions*; Camps, M., Szmids, C., Eds.; Oxbow Books: Oxford, UK, 2009; pp. 293–311.
7. Jöris, O.; Álvarez Fernández, E.; Weninger, B. Radiocarbon evidence of the Middle to Upper Palaeolithic transition in Southwestern Europe. *Trab. Prehist.* **2003**, *60*, 15–38. [[CrossRef](#)]
8. Finlayson, C.; Giles Pacheco, F.; Rodríguez-Vidal, J.; Fa, D.A.; María Gutierrez López, J.; Santiago Pérez, A.; Finlayson, G.; Allue, E.; Baena Preysler, J.; Cáceres, I.; et al. Late survival of Neanderthals at the southernmost extreme of Europe. *Nature* **2006**, *443*, 850–853. [[CrossRef](#)] [[PubMed](#)]
9. Finlayson, C.; Fa, D.A.; Jiménez Espejo, F.; Carrión, J.S.; Finlayson, G.; Giles Pacheco, F.; Rodríguez Vidal, J.; Stringer, C.; Martínez Ruiz, F. Gorham's Cave, Gibraltar—The persistence of a Neanderthal population. *Quat. Int.* **2008**, *181*, 64–71. [[CrossRef](#)]
10. Zilhão, J.; Davis, S.J.M.; Duarte, C.; Soares, A.M.M.; Steier, P.; Wild, E. Pego do Diabo (Loures, Portugal): Dating the emergence of anatomical modernity in westernmost Eurasia. *PLoS ONE* **2010**, *5*, e8880. [[CrossRef](#)]
11. Zilhão, J.; Anesin, D.; Aubry, T.; Badal, E.; Cabanes, D.; Kehl, M.; Klasen, N.; Lucena, A.; Martín-Lerma, I.; Martínez, S.; et al. Precise dating of the Middle-to-Upper Paleolithic transition in Murcia (Spain) supports late Neanderthal persistence in Iberia. *Heliyon* **2017**, *3*, e00435. [[CrossRef](#)]
12. Bradtmöller, M.; Pastoors, A.; Weninger, B.; Weniger, G.-C.C. The repeated replacement model—Rapid climate change and population dynamics in Late Pleistocene Europe. *Quat. Int.* **2012**, *247*, 38–49. [[CrossRef](#)]
13. De la Peña, P. The beginning of the Upper Paleolithic in the Baetic Mountain area (Spain). *Quat. Int.* **2013**, *318*, 69–89. [[CrossRef](#)]
14. Galván, B.; Hernández, C.M.; Mallol, C.; Mercier, N.; Sistiaga, A.; Soler, V. New evidence of early Neanderthal disappearance in the Iberian Peninsula. *J. Hum. Evol.* **2014**, *75*, 16–27. [[CrossRef](#)] [[PubMed](#)]
15. Bicho, N.; Marreiros, J.; Cascalheira, J.; Pereira, T.; Haws, J. Bayesian modeling and the chronology of the Portuguese Gravettian. *Quat. Int.* **2015**, *359–360*, 499–509. [[CrossRef](#)]
16. Santonja, M.; Pérez-González, A. La industria lítica del miembro estratigráfico medio de Ambrona (Soria, España) en el contexto del Paleolítico Antiguo de la Península Ibérica. *Zephyros* **2006**, *59*, 7–20.
17. Terradillos-Bernal, M.; Díez-Fernández-Lomana, J.C. La transition entre les Modes 2 et 3 en Europe: Le rapport sur les gisements du Plateau Nord (Péninsule Ibérique). *Anthropologie* **2012**, *116*, 348–363. [[CrossRef](#)]
18. Ollé, A.; Mosquera, M.; Rodríguez, X.P.; de Lombra-Hermida, A.; García-Antón, M.D.; García-Medrano, P.; Peña, L.; Menéndez, L.; Navazo, M.; Terradillos, M.; et al. The Early and Middle Pleistocene technological record from Sierra de Atapuerca (Burgos, Spain). *Quat. Int.* **2013**, *295*, 138–167. [[CrossRef](#)]
19. Álvarez-Alonso, D. First Neanderthal settlements in northern Iberia: The acheulean and the emergence of mousterian technology in the Cantabrian region. *Quat. Int.* **2014**, *326–327*, 288–306. [[CrossRef](#)]
20. Santonja, M.; Pérez-González, A.; Panera, J.; Rubio-Jara, S.; Méndez-Quintas, E. The coexistence of Acheulean and Ancient Middle Palaeolithic techno-complexes in the Middle Pleistocene of the Iberian Peninsula. *Quat. Int.* **2016**, *411*, 367–377. [[CrossRef](#)]
21. Daura, J.; Sanz, M.; Arsuaga, J.L.; Hoffmann, D.L.; Quam, R.M.; Ortega, M.C.; Santos, E.; Gómez, S.; Rubio, Á.; Villaescusa, L.; et al. New Middle Pleistocene hominin cranium from Gruta da Aroeira (Portugal). *Proc. Natl. Acad. Sci. USA* **2017**, *114*, 3397–3402. [[CrossRef](#)]
22. Pereira, T.; Cunha, P.P.; Martins, A.A.; Nora, D.; Paixão, E.; Figueiredo, O.; Raposo, L.; Henriques, F.; Caninas, J.; Moura, D.; et al. Geoarchaeology of the Cobrinhos site (Vila Velha de Ródão, Portugal)—A record of the earliest Mousterian in western Iberia. *J. Archaeol. Sci. Rep.* **2019**, in press.

23. Cunha, P.P. Estratigrafia e Sedimentologia dos Depósitos do Cretácico Superior e Terciário de Portugal Central, a Leste de Coimbra/Stratigraphy and Sedimentology of the Upper Cretaceous and Tertiary of Central Portugal, East of Coimbra. Ph.D. Thesis, University of Coimbra, Coimbra, Portugal, July 1992.
24. Cunha, P.P.; Barbosa, B.P.; Pena dos Reis, R. Synthesis of the Piacenzian onshore record, between the Aveiro and Setúbal parallels (Western Portuguese margin). *Ciências da Terra* **1993**, *12*, 35–43.
25. Cunha, P.P. Unidades litostratigráficas do Terciário da Beira Baixa (Portugal). *Comum. Inst. Geol. Min.* **1996**, *82*, 87–130.
26. Cunha, P.P.; Martins, A.A.; Huot, S.; Murray, A.S.; Raposo, L. Dating the Tejo River lower terraces in the Ródão area (Portugal) to assess the role of tectonics and uplift. *Geomorphology* **2008**, *102*, 43–54. [[CrossRef](#)]
27. Cunha, P.P.; Martins, A.A.; Gouveia, M.P. As escadarias de terraços do Ródão à Chamusca (Baixo Tejo)—Caracterização e interpretação de dados sedimentares, tectónicos, climáticos e do Paleolítico/The terrace staircases of the Lower Tagus River (Ródão to Chamusca)—Characterization and interpretation of the sedimentary, tectonic, climatic and Palaeolithic data. *Estudos do Quaternário* **2016**, *14*, 1–24. [[CrossRef](#)]
28. Cunha, P.P.; Martins, A.A.; Buylaert, J.P.; Murray, A.S.; Raposo, L.; Mozzi, P.; Stokes, M. New data on the chronology of the Vale do Forno sedimentary sequence (Lower Tejo River terrace staircase) and its relevance as a fluvial archive of the Middle Pleistocene in western Iberia. *Quat. Sci. Rev.* **2017**, *166*, 204–226. [[CrossRef](#)]
29. Almeida, N.; Deprez, S.; De Dapper, M. The Palaeolithic occupation of the Northeastern of Alen Tagus (Portugal): A geoarchaeological approach. In *Graphical Markers and Megalith Builders in the International Tagus, Iberian Peninsula—British Archaeological Reports International Series*; Bueno-Ramirez, P., Barroso-Bermejo, R., Balbín Berhmann, R., Eds.; Archaeopress: Oxford, UK, 2008; Volume 1765, pp. 19–26. ISBN 9781407302546.
30. Stokes, M.; Cunha, P.P.; Martins, A.A. Techniques for analysing Late Cenozoic river terrace sequences. *Geomorphology* **2012**, *165–166*, 1–6. [[CrossRef](#)]
31. Duller, G.A.T. Luminescence dating of Quaternary sediments: Recent advances. *J. Quat. Sci.* **2004**, *19*, 183–192. [[CrossRef](#)]
32. Murray, A.; Marten, R.; Johnston, A.; Martin, P. Analysis for naturally occurring radionuclides at environmental concentrations by gamma spectrometry. *J. Radioanal. Nucl. Chem.* **1987**, *115*, 263–288. [[CrossRef](#)]
33. Olley, J.M.; Murray, A.S.; Roberts, R.G. The effects of disequilibria in the uranium and thorium decay chains on burial dose rates in fluvial sediments. *Quat. Sci. Rev.* **1996**, *15*, 751–760. [[CrossRef](#)]
34. Huntley, D.J.; Baril, M.R. The K content of the K-feldspars being measured in optical dating or in thermoluminescence dating. *Ancient TL* **1997**, *15*, 11–13.
35. Thomsen, K.J.; Murray, A.S.; Jain, M.; Bøtter-Jensen, L. Laboratory fading rates of various luminescence signals from feldspar-rich sediment extracts. *Radiat. Meas.* **2008**, *43*, 1474–1486. [[CrossRef](#)]
36. Buylaert, J.-P.; Jain, M.; Murray, A.S.; Thomsen, K.J.; Thiel, C.; Sohbati, R. A robust feldspar luminescence dating method for Middle and Late Pleistocene sediments. *Boreas* **2012**, *41*, 435–451. [[CrossRef](#)]
37. Kruiver, P.P.; Dekkers, M.J.; Heslop, D. Quantification of magnetic coercivity components by the analysis of acquisition curves of isothermal remanent magnetisation. *Earth Planet. Sci. Lett.* **2001**, *189*, 269–276. [[CrossRef](#)]
38. Costa, F.G.C.M.; Bove, C.P.; Arruda, R.; Philbrick, C.T. Silica bodies and their systematic implications at the subfamily level in Podostemaceae. *Rodriguesia* **2011**, *62*, 937–942. [[CrossRef](#)]
39. Piperno, D.R. *Phytoliths: A Comprehensive Guide for Archaeologists and Paleoecologists*; Rowman Altamira Press: Oxford, UK, 2006; p. 238. ISBN 9780759103856.
40. Twiss, P.C.; Suess, E.; Smith, R.M. Morphological classification of grass phytoliths. *Soil Sci. Soc. Am. Proc.* **1969**, *33*, 109–115. [[CrossRef](#)]
41. Madella, M.; Alexandre, A.; Ball, T. International code for phytolith nomenclature 1.0. *Ann. Bot.* **2005**, *96*, 253–260. [[CrossRef](#)] [[PubMed](#)]
42. Faegri, K.; Iversen, J. *Textbook of Pollen Analysis*, 4th ed.; Faegri, K., Kaland, P.E., Krzywinski, K., Eds.; John Wiley and Sons: Chichester, UK, 1989; ISBN 0 471 92178 5.
43. Moore, P.D.; Webb, J.A.; Collinson, M.E. *Pollen Analysis*; Blackwell: Oxford, UK, 1991; 216p, ISBN 0632021764.
44. Reille, M. *Pollen et Spores d'Europe et d' Afrique du Nord*; Laboratoire de Botanique Historique et Palynologie: Marseille, France, 1992; 543p, ISBN 2-9507175-0-0.
45. Reille, M. *Pollen et Spores d'Europe et d' Afrique du Nord*; Supplement 1; Laboratoire de Botanique Historique et Palynologie: Marseille, France, 1995; ISBN 2950717519.

46. Reille, M. *Pollen et Spores d'Europe et d'Afrique du Nord*; Laboratoire de Botanique Historique et Palynologie: Marseille, France, 1999; ISBN-10: 2950717535.
47. Wintle, A.G.; Murray, A.S. A review of quartz optically stimulated luminescence characteristics and their relevance in single-aliquot regeneration dating protocols. *Radiat. Meas.* **2006**, *41*, 369–391. [[CrossRef](#)]
48. Raposo, L. Ambientes, Territórios y Subsistencia en el Paleolítico Medio de Portugal. *Complutum* **1995**, *6*, 57–78.
49. Thompson, R.; Oldfield, F. *Environmental Magnetism*; Allen and Unwin: London, UK, 1986; p. 227.
50. Evans, M.E.; Heller, F. *Environmental Magnetism: Principles and Applications of Enviromagnetics*; Academic: San Diego, CA, USA, 2003; ISBN 9780080505787.
51. Grygar, T.; Svetlik, I.; Lisa, L.; Koptikova, L.; Bajer, A.; Wray, D.S.; Ettler, V.; Mihaljevic, M.; Novakova, T.; Koubova, M.; et al. Geochemical tools for the stratigraphic correlation of floodplain deposits of the Morava River in Straznické Pomoravi, Czech Republic from the last millennium. *Catena* **2010**, *80*, 106–121. [[CrossRef](#)]
52. Desenfant, F.; Petrovsky, E.; Rochette, P. Magnetic signature of industrial pollution of stream sediments and correlation with heavy metals: Case study from South France. *Water Air Soil Pollut.* **2004**, *152*, 297–312. [[CrossRef](#)]
53. Zhang, C.X.; Appel, E.; Qiao, Q.Q. Heavy metal pollution in farmland irrigated with river water near a steel plant—magnetic and geochemical signature. *Geophys. J. Int.* **2013**, *192*, 963–974. [[CrossRef](#)]
54. Maher, B.A.; Thompson, R. Pedogenesis and Paleoclimate—Interpretation of the Magnetic-Susceptibility Record of Chinese Loess-Paleosol Sequences—Comment. *Geology* **1994**, *22*, 857–858. [[CrossRef](#)]
55. Maher, B.A.; Alekseev, A.; Alekseeva, T. Magnetic mineralogy of soils across the Russian Steppe: Climatic dependence of pedogenic magnetite formation. *Palaeogeogr. Palaeoclimatol. Palaeoecol.* **2003**, *201*, 321–341. [[CrossRef](#)]
56. Egli, R. Characterization of Individual Rock Magnetic Components by Analysis of Remanence Curves, 1. Unmixing Natural Sediments. *Studia Geophysica et Geodaetica* **2004**, *48*, 391–446. [[CrossRef](#)]
57. Cunha, P.P.; Cura, S.; Cunha Ribeiro, J.P.; Figueiredo, S.; Martins, A.A.; Raposo, L.; Pereira, T.; Almeida, N. As indústrias do Paleolítico Inferior e Médio associadas ao Terraço T4 do Baixo Tejo (Portugal central)—Arquivos da mais antiga ocupação humana no oeste da Ibéria, com ca. 340 ka a 155 ka/The Lower and Middle Palaeolithic industries associated with the T4 Terrace of the Lower Tejo River—Archives of the human occupation during ca. 335 ka to 155 ka ago. *J. Lithic Stud.* **2017**, *4*, 27–56. [[CrossRef](#)]
58. Raposo, L. Os mais antigos vestígios de ocupação humana paleolítica na região de Ródão. In *Da Pré-História, Homenagem a O. Veiga Ferreira*; Editorial Delta: Madrid, Spain, 1987; pp. 153–178.
59. Silva, A.; Pimenta, C.; Lemos, F.; Zilhão, J.; Mateus, J.; Raposo, L.; Coutinho, M. Vilas Ruivas: Um acampamento do Paleolítico Médio. *História e Sociedade* **1980**, *7*, 29–33.
60. Raposo, L.; Silva, A.C. A estação Paleolítica de Vilas Ruivas (Ródão). Campanha de 1979. *O Arqueólogo Português* **1993**, *IV*, 15–38.
61. Almeida, N.A.C. Estruturas de habitat do final do Plistocénico médio em Portugal: O caso dos Pegos do Tejo 2, Portas de Ródão, Nisa. In *Arqueologia Em Portugal—150 Anos*; Associação dos Arqueólogos Portugueses: Lisboa, Portugal, 2013; pp. 243–250.
62. Almeida, N.A.C. O Paleolítico Médio das Portas de Ródão, a Margem Esquerda (Nisa, Portugal). Contributo para a sua Caracterização Cronoestratigráfica. Ph.D Thesis, Universidade de Évora, Évora, Portugal, January 2014.
63. Monteiro, M.; Henriques, F.; Clélia, S.; Évora, M.; Nora, D.; Alves, C.; Mendes, C.; Carvalho, E.; Anacleto, C.; Silva, D.; et al. Monte da Revelada 2—Resultados preliminares. *AÇAFA On-line* **2017**, *11*, 18–27.
64. Raposo, L. Campanha de Escavações Arqueológicas no Sítio da Foz do Enxarrique. Alto Tejo. *Boletim Informativo do Núcleo Regional de Investigação Arqueológica* **1991**, *9*, 1–2.
65. Cardoso, J.L. *Contribuição para o conhecimento dos grandes mamíferos do Plistocénico Superior de Portugal*; Câmara Municipal de Oeiras: Oeiras, Portugal, 1993.
66. Brugal, J.-P.; Raposo, L. Foz do Enxarrique (Ródão—Portugal): Preliminary results of the analysis of a bone assemblage from A Middle Palaeolithic open site. In *The Role of Early Humans in the Accumulation of European Lower and Middle Palaeolithic Bone Assemblages*; Römisch Germanisches Zentralmuseum Mainz: Mainz, Germany, 1999; pp. 367–379. ISBN 9783884670446.
67. Sousa, M.F.; Figueiredo, S.D. The Pleistocene Elephants of Portugal. In *Proceedings of the Congresso La Terra degli Elefanti (Actas)*, Roma, Italy, 16–20 October 2001; pp. 611–616.

68. Figueiredo, S.D.; Sousa, M.F. Os Elefantes Pleistocénicos de Portugal. *Revista Evolução* **2003**, *1*, 3–32.
69. Figueiredo, S.D.; Raposo, L. As Aves Como Recurso Alimentar do Homem do Paleolítico Médio: Interpretação tafonómica das acumulações faunísticas da Gruta Nova da Columbeira e da Foz do Enxarrique. *Boletim do Centro Português de Geo-História e Pré-História* **2018**, *4*, 69–82.
70. Berruti, G.L.F.; Rosina, P.; Raposo, L. The use-wear analysis of the quartzite lithic assemblage from the middle Palaeolithic site of Foz do Enxarrique (Ródão, Portugal). *Mediterr. Archaeol. Archaeom.* **2016**, *16*, 107–126. [[CrossRef](#)]
71. Marín-Arroyo, A.B.; Rios-Garaizar, J.; Straus, L.G.; Jones, J.R.; de la Rasilla, M.; González Morales, M.R.; Richards, M.; Altuna, J.; Mariezkurrena, K.; Ocio, D. Chronological reassessment of the Middle to Upper Paleolithic transition and Early Upper Paleolithic cultures in Cantabrian Spain. *PLoS ONE* **2018**, *13*, e0194708. [[CrossRef](#)]
72. Zilhão, J. Middle Paleolithic settlement patterns in Portugal. In *Settlement Dynamics of the Middle Paleolithic and Middle Stone Age*; Conard, N., Ed.; Kerns Verlag: Tübingen, Germany, 2001; pp. 597–608.
73. Cardoso, J.L. The Mousterian complex in Portugal. *Zephyrus* **2006**, *59*, 21–50.
74. Benedetti, M.M.; Haws, J.A.; Funk, C.L.; Daniels, J.M.; Hesp, P.A.; Bicho, N.F.; Minckley, T.A.; Ellwood, B.B.; Forman, S.L. Late Pleistocene raised beaches of coastal Estremadura, central Portugal. *Quat. Sci. Rev.* **2009**, *28*, 3428–3447. [[CrossRef](#)]
75. Pereira, T.; Bicho, N.; Haws, J. O Paleolítico Médio em Território Português. *Mainake* **2012**, *33*, 11–30.
76. Martignier, L.; Nussbaumer, M.; Adatte, T.; Gobat, J.M.; Verrecchia, E.P. Assessment of a locally—Sourced loess system in Europe: The Swiss Jura Mountains. *Aeolian Res.* **2015**, *18*, 11–21. [[CrossRef](#)]
77. Újvári, G.; Kok, J.F.; Varga, G.; Kovács, J. The physics of wind-blown loess: Implications for grain size proxy interpretations in Quaternary paleoclimate studies. *Earth-Sci. Rev.* **2016**, *154*, 247–278. [[CrossRef](#)]
78. Vandenberghe, J.; Sun, Y.; Wang, X.; Abels, H.A.; Liu, X. Grain-size characterization of reworked fine-grained aeolian deposits. *Earth-Sci. Rev.* **2018**, *177*, 43–52. [[CrossRef](#)]
79. Varga, G.; Újvári, G.; Kovács, J. Interpretation of sedimentary (sub)populations extracted from grain size distributions of Central European loess-paleosol series. *Quat. Int.* **2017**. [[CrossRef](#)]
80. Wolf, D.; Ryborz, K.; Kolb, T.; Calvo Zapata, R.; Sanchez Vizcaino, J.; Zöller, L.; Faust, D. Origins and genesis of loess deposits in central Spain, as indicated by heavy mineral compositions and grain-size variability. *Sedimentology* **2018**, in press. [[CrossRef](#)]
81. Kravchinsky, V.A.; Langereis, C.G.; Walker, S.D.; Dlusskiy, K.G.; White, D. Discovery of Holocene millennial climate cycles in the Asian continental interior: Has the sun been governing the continental climate? *Glob. Planet. Chang.* **2013**, *110*, 386–396. [[CrossRef](#)]
82. Liu, Q.S.; Deng, C.L.; Yu, Y.J.; Torrent, J.; Jackson, M.J.; Banerjee, S.K.; Zhu, R.X. Temperature dependence of magnetic susceptibility in an argon environment: Implications for pedogenesis of Chinese loess/palaeosols. *Geophys. J. Int.* **2005**, *161*, 102–112. [[CrossRef](#)]
83. Maher, B.A. The magnetic properties of Quaternary aeolian dusts and sediments, and their palaeoclimatic significance. *Aeolian Res.* **2011**, *3*, 87–144. [[CrossRef](#)]
84. Shi, L.F.; Yang, Z.Y.; Zheng, L.D.; Jia, S.M.; Tong, Y.B.; Zhang, S.Q.; Xu, D.Y.; Guo, G.X. Environmental magnetic record of the fluvial sediments from the Tianzhu borehole in Beijing for the last 800 ka. *Earth Planets Space* **2010**, *62*, 631–645. [[CrossRef](#)]
85. Lu, H.Y.; Van Huissteden, K.O.; An, Z.S.; Nugteren, G.; Vandenberghe, J. East Asia winter monsoon variations on a millennial time-scale before the last glacial-interglacial cycle. *J. Quat. Sci.* **1999**, *14*, 101–110. [[CrossRef](#)]
86. Maher, B.A.; Thompson, R. Paleoclimatic significance of the mineral magnetic record of the Chinese loess and paleosols. *Quat. Res.* **1992**, *37*, 155–170. [[CrossRef](#)]
87. Maher, B.A. Environmental magnetism and climate change. *Contemp. Phys.* **2007**, *48*, 247–274. [[CrossRef](#)]
88. Sánchez Goñi, M.F.; Eynaud, F.; Turon, J.L.; Shackleton, N.J. High resolution palynological record off the Iberian Margin: Direct land-sea correlation for the Last Interglacial complex. *Earth Planet. Sci. Lett.* **1999**, *171*, 123–137. [[CrossRef](#)]
89. Sánchez Goñi, M.F.; Turon, J.-L.; Eynaud, F.; Gendreau, S. European climatic response to millennial-scale changes in the atmosphere-ocean system during the last glacial period. *Quat. Res.* **2000**, *54*, 394–403. [[CrossRef](#)]

90. Sánchez Goñi, M.F.; Cacho, I.; Turon, J.-L.; Guiot, J.; Sierro, F.J.; Peyrouquet, J.-P.; Grimalt, J.O.; Shackleton, N.J. Synchronicity between marine and terrestrial responses to millennial scale climatic variability during the last glacial period in the Mediterranean region. *Climate Dyn.* **2002**, *19*, 95–105. [[CrossRef](#)]
91. Roucoux, K.H.; Shackleton, N.J.; de Abreu, L.; Schönfeld, J.; Tzedakis, P.C. Combined marine proxy and pollen analyses reveal rapid Iberian vegetation response to North Atlantic millennial-scale climate oscillations. *Quat. Res.* **2001**, *56*, 128–132. [[CrossRef](#)]
92. Roucoux, K.H.; de Abreu, L.; Shackleton, N.J.; Tzedakis, P.C. The response of NW Iberian vegetation to North Atlantic climate oscillations during the last 65 kyr. *Quat. Sci. Rev.* **2005**, *24*, 1637–1653. [[CrossRef](#)]
93. De Abreu, L.; Shackleton, N.J.; Schönfeld, J.; Hall, M.; Chapman, M.R. Millennial-scale oceanic climate variability off the Western Iberian margin during the last two glacial periods. *Mar. Geol.* **2003**, *196*, 1–20. [[CrossRef](#)]
94. Schönfeld, J.; Zahn, R.; de Abreu, L. Surface to deep water response to rapid climate changes at the western Iberian Margin. *Glob. Planet. Chang.* **2003**, *36*, 237–264. [[CrossRef](#)]
95. Dansgaard, W.; Johnsen, S.J.; Clauuser, H.B.; Dahl, J.; Gundestrup, N.S.; Hommer, C.U.; Huidberg, C.S.; Steffensen, J.P.; Svernbjornsdottir, A.E.; Jouzel, J.; et al. Evidence for general instability of past climate from a 250 kyr ice-core record. *Nature* **1993**, *364*, 218–220. [[CrossRef](#)]
96. Grootes, P.M.; Stuiver, M.; White, J.W.C.; Johnsen, S.; Jouzel, J. Comparison of oxygen isotope records from the GISP2 and GRIP Greenland ice cores. *Nature* **1993**, *366*, 552–554. [[CrossRef](#)]
97. Ruiz Zapata, M.B.; Rodríguez de Tembleque, J.M.; Pérez González, A.; Gil García, M.J. Paleovegetación en el yacimiento achelense de Puente Pino y su entorno (Toledo, España). *Cuaternario y Geomorfología* **2009**, *23*, 113–126.



© 2019 by the authors. Licensee MDPI, Basel, Switzerland. This article is an open access article distributed under the terms and conditions of the Creative Commons Attribution (CC BY) license (<http://creativecommons.org/licenses/by/4.0/>).